Cellular and Molecular Life Sciences (2021) 78:8187–8208
https://doi.org/10.1007/s00018-021-03981-w

ORIGINAL ARTICLE

A survey of substrate specificity among Auxiliary Activity Family 5 copper radical oxidases

Maria E. Cleveland[1,2,3] · Yann Mathieu[1,3] · David Ribeaucourt[4,5,6] · Mireille Haon[4] · Paul Mulyk[2] · Jason E. Hein[2] · Mickael Lafond[5] · Jean-Guy Berrin[4] · Harry Brumer[1,2,3,7,8]

Received: 20 July 2021 / Revised: 13 September 2021 / Accepted: 13 October 2021 / Published online: 5 November 2021

Abstract

There is significant contemporary interest in the application of enzymes to replace or augment chemical reagents toward the development of more environmentally sound and sustainable processes. In particular, copper radical oxidases (CRO) from Auxiliary Activity Family 5 Subfamily 2 (AA5_2) are attractive, organic cofactor-free catalysts for the chemoselective oxidation of alcohols to the corresponding aldehydes. These enzymes were first defined by the archetypal galactose-6-oxidase (GalOx, EC 1.1.3.13) from the fungus *Fusarium graminearum*. The recent discovery of specific alcohol oxidases (EC 1.1.3.7) and aryl alcohol oxidases (EC 1.1.3.47) within AA5_2 has indicated a potentially broad substrate scope among fungal CROs. However, only relatively few AA5_2 members have been characterized to date. Guided by sequence similarity network and phylogenetic analysis, twelve AA5_2 homologs have been recombinantly produced and biochemically characterized in the present study. As defined by their predominant activities, these comprise four galactose 6-oxidases, two raffinose oxidases, four broad-specificity primary alcohol oxidases, and two non-carbohydrate alcohol oxidases. Of particular relevance to applications in biomass valorization, detailed product analysis revealed that two CROs produce the bioplastics monomer furan-2,5-dicarboxylic acid (FDCA) directly from 5-hydroxymethylfurfural (HMF). Furthermore, several CROs could desymmetrize glycerol (a by-product of the biodiesel industry) to D- or L-glyceraldehyde. This study furthers our understanding of CROs by doubling the number of characterized AA5_2 members, which may find future applications as biocatalysts in diverse processes.

Keywords Copper radical oxidase · Alcohol oxidase · Galactose oxidase · Biocatalysis · Auxiliary Activity Family 5

✉ Harry Brumer
brumer@msl.ubc.ca

1 Michael Smith Laboratories, University of British Columbia, 2185 East Mall, Vancouver, BC V6T 1Z4, Canada

2 Department of Chemistry, University of British Columbia, 2036 Main Mall, Vancouver, BC V6T 1Z1, Canada

3 BioProducts Institute, University of British Columbia, 2385 East Mall, Vancouver, BC V6T 1Z4, Canada

4 INRAE, Aix Marseille Univ, UMR 1163 Biodiversité et Biotechnologie Fongiques, 13009 Marseille, France

5 Aix Marseille Univ, CNRS, Centrale Marseille, iSm2, Marseille, France

6 V. Mane Fils, 620 route de Grasse, 06620 Le Bar sur Loup, France

7 Department of Biochemistry and Molecular Biology, University of British Columbia, 2350 Health Sciences Mall, Vancouver, BC V6T 1Z3, Canada

8 Department of Botany, University of British Columbia, 3200 University Boulevard, Vancouver, BC V6T 1Z4, Canada

Introduction

Global climate change due to human activities is a pressing issue confronting our society (https://climate.nasa.gov/scientific-consensus/) [1]. One avenue to decrease reliance on petroleum is to increase the utilization of plant biomass as a renewable carbon feedstock [2, 3]. Plant biomass is an abundant source of complex polysaccharides, polyaromatics (i.e., lignin), and low molecular weight extractives (e.g., lipids, terpenes, etc.), each of which can potentially be valorized via (bio)catalytic routes. Foremost, the development of the so-called "biofuels," e.g., ethanol fermented from sugar feedstocks, has received the widest attention, but faces certain economic and scalability challenges [4–6]. In parallel, there is a growing appreciation that upgrading plant biomass components to produce high-value biochemicals and biomaterials may provide solutions to lower reliance on fossil petroleum beyond the energy sector [7–11].

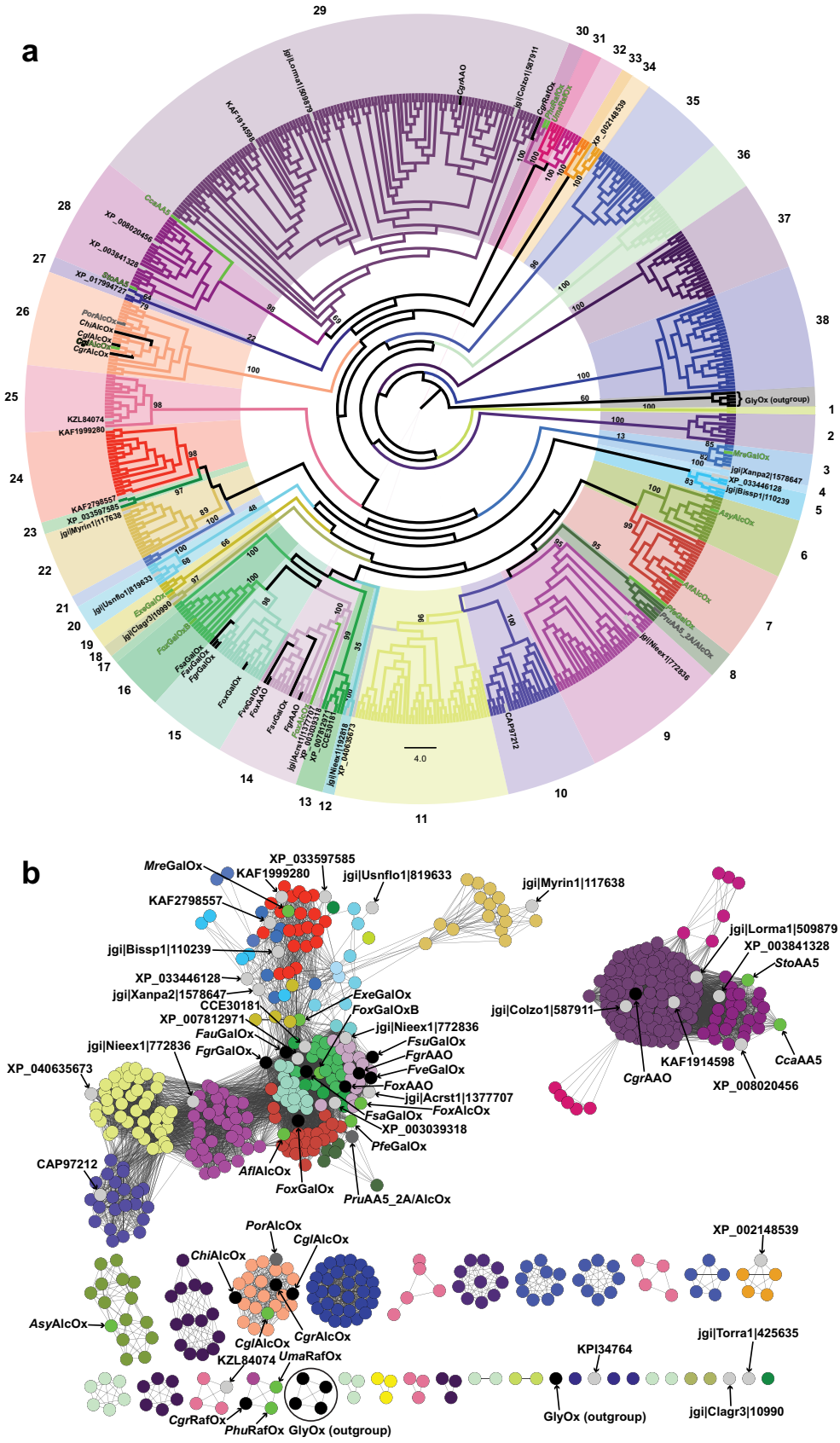
a
b
GlyOx (outgroup)
MreGalOx
AsyAlcOx
AflAlcOx
PruAA5_2A/AlcOx
FoxGalOx
FoxAAO
FoxAlcOx
FsaGalOx
PfeGalOx
FgrAAO
FveGalOx
FauGalOx
FgrGalOx
ExeGalOx
FoxGalOxB
FsuGalOx
FveAAO
FoxAAO
PorAlcOx
CglAlcOx
ChiAlcOx
CgrAlcOx
UmaRafOx
PhuRafOx
CgrRafOx
StoAA5
CcaAA5
CgrAAO
KAF1914598
XP_008020456
XP_002148539
jgi|Torra1|425635
KPI34764
jgi|Clagr3|10990
jgi|Lorma1|509879
XP_003841328
jgi|Colzo1|587911
jgi|Myrin1|117638
jgi|Usnflo1|819633
jgi|Bissp1|110239
jgi|Xanpa2|1578647
XP_033446128
XP_033597585
KAF2798557
KAF1999280
jgi|Nieex1|772836
XP_040635673
CAP97212
jgi|Acrst1|1377707
XP_003039318
KZL84074

◂**Fig. 1** Sequence relationships of 623 AA5_2 catalytic modules. **a** Phylogenetic tree with bootstrap values supporting the 38 subgroups are indicated at each node/branch. For branches exhibiting low bootstrap values (< 50), values supporting the nodes are indicated. **b** Sequence similarity network (SSN). Each node corresponds to one of the 623 catalytic modules used as an input to build the SSN created in Cytoscape with yFiles Organic layout [104]. Edges represent an alignment bit score threshold of 550, which clusters the sequences into groups analogous to those observed in (**a**) and color coded accordingly. In both panels, AA5 members with previously available biochemical data are colored in black and indicated as (methyl)glyoxal oxidases (*Uma*GlyOx [67], *Pch*GlyOx1 and *Pch*GlyOx2 [68], *Pci*GlyOx1 and *Pci*GlyOx2 [110]) (comprising the outgroup), galactose oxidases (*Fgr*GalOx [66, 73, 92], *Fox*GalOx [65], *Fsa*GalOx [64], *Fsu*GalOx [63], *Fve*GalOx, and *Fsu*GalOx [111]), alcohol oxidases (*Cgr*AlcOx and *Cgl*AlcOx [37], *Chi*AlcOx and *Por*AlcOx [38], raffinose oxidase (*Cgr*RafOx) [62], AA5_2 oxidase (*Pru*AA5_2A (*Pru*AlcOx)) [61], and the aryl alcohol oxidase (*Cgr*AAO) [39]. Enzymes first characterized in the present study are colored in neon green. Two selected sequences for which characterization was published contemporaneously, *Pru*AA5_2A (*Pru*AlcOx) [61] and *Por*AlcOx [38], are colored in grey

The utilization of plant biomass poses many challenges due to inherent chemical and structural complexity, which make fractionation and chemical transformation difficult. Yet, a wide diversity of microorganisms have developed specialized biocatalytic systems of hydrolytic and oxidative enzymes to unlock this natural resource [12–22]. Informed by decades of fundamental biochemical research [23–26], industrial enzyme "cocktails" have been developed for complete saccharification of plant biomass, especially starch and cellulose fractions, for fermentation to biofuels [27–29]. Spurred by a growing track record of successful applications and significant industrial infrastructure for scalable production, enzyme-based biocatalysis is enjoying a period of sustained and growing interest [30–32]. In particular, there is strong demand to replace chemical oxidants, many of which produce hazardous waste, with "greener" alternatives, making the study of oxidative enzymes attractive in this context [14, 32].

One class of oxidases that has shown promise for the valorization of plant biomass is the copper radical oxidases (CROs) that comprise Auxiliary Activity Family 5 (AA5) in the Carbohydrate-Active Enzymes (CAZy) classification [17]. These enzymes contain a mono-nuclear copper radical center coordinated by a distinct crosslinked tyrosine-cysteine active-site residue, which catalyzes two one-electron oxidations with concomitant reduction of oxygen to hydrogen peroxide [33, 34]. Within AA5, two subfamilies have been identified: Characterized subfamily 1 (AA5_1) enzymes have predominant activity on glyoxal and methylglyoxal (GlyOx, EC 1.2.3.15) [35]. Subfamily 2 (AA5_2) contains the archetypal CRO, galactose 6-oxidase (GalOx, EC 1.1.3.9) [33, 36], as well as the more recently discovered general alcohol oxidases (AlcOx, EC 1.1.3.13) [37, 38], and aryl alcohol oxidases (AAO, EC 1.1.3.7) [39, 40]. Both AA5_1 and AA5_2 have been speculated to be involved in the oxidative degradation of lignocellulose [34]; however, recently, AA5_2 alcohol oxidases have been linked to oxidizing plant cuticular long-chain alcohols into aldehyde products during fungal infection [41].

The archetypal galactose oxidase from the phytopathogenic fungus *Fusarium graminearum* (*Fgr*GalOx) and its engineered variants have found widespread biotechnological applications, including in glycoprotein labeling, biosensor development, polysaccharide functionalization, and other applications involving the oxidation of carbohydrates or other alcohols [42–54]. Of particular note, a highly evolved variant of *Fgr*GalOx was utilized recently in the biocatalytic synthesis of the HIV drug islatravir [55]. Furthermore, *Cgr*AlcOx has been demonstrated to be a promising green catalyst for the oxidation of long-chain aliphatic alcohols for the production of flavor and fragrance compounds [56], whereas *Cgr*AAO has been shown to be effective at oxidizing HMF, which is important in the context of biopolymer manufacturing [39, 57, 58]. Thus, there is sustained interest to expand the utilization of CROs industrially, through the discovery of homologs with inherently diverse catalytic specificities [14, 59, 60].

However, very few (currently thirteen) CROs from AA5_2 have been biochemically characterized [37–40, 61–66], the majority of which originate from two fungal genera: *Fusarium* [33, 40, 63–65] and *Colletotrichum* [37–39, 62] (for an updated list see http://www.cazy.org/AA5_characterized.html, [17]). Nonetheless, recent studies have revealed homologs in these fungi with distinct specificities for alkyl and aryl alcohols, indicating that the large sequence space of uncharacterized AA5 members presents an opportunity to uncover new biocatalysts [37, 39, 40, 60]. Inspired by these results, we were keen to continue mapping activities across the AA5_2 subfamily, drawing upon a growing array of new fungal genomes.

Hence, in the present study we have combined molecular phylogeny and sequence similarity network analysis to guide the selection of 40 AA5_2 members from diverse fungi for recombinant expression in the yeast *Pichia pastoris*. Fourteen of these were successfully produced and twelve were fully biochemically characterized, revealing new galactose 6-oxidases, raffinose oxidases, broad-specificity primary alcohol oxidases, and non-carbohydrate alcohol oxidases.

Results

Phylogeny of the AA5_2 subfamily

A manually curated multiple protein sequence alignment of over 623 AA5_2 catalytic modules, with signal peptides and additional domains removed, was used to generate a

Maximum Likelihood (ML) phylogeny and a sequence similarity network (SSN) (Fig. 1). Using AA5_1 glyoxal oxidases [67, 68] as an outgroup, 38 subgroups were identified based on tree topology and generally high supporting bootstrap values (Fig. 1A). As indicated, the previously characterized AA5_2 members are broadly dispersed in the tree, with some enzymes clustered into more well-represented clades. Specifically, GalOxs are located in clade 15, general AlcOxs cluster into clade 26, while AAOs are found in clade 14 and clade 29 (Fig. 1). The corresponding SSN at an alignment score (bit score) cut-off of 550 was consistent with the grouping observed in the phylogenetic tree and subsequently used to aid sequence selection and mapping of biochemical data (Fig. 1B). In Table 1 and subsequently in the text, the targets are named according to their predominant activities as determined by subsequent kinetic assays (*vide infra*).

To further inform target selection, we mapped the variability of the amino acids involved in catalysis and substrate recognition, as determined by mutagenesis and/or structural analysis of AA5_2 members [69–77], onto the SSN (Table 1, Table S1 Figure S1). Thus, 40 targets were selected to represent the maximum diversity of sequence identity and fungal ecology, such as saprotrophic and phytopathogenic members, in this sample size (Table 1 and Figure S1).

Table 1 Key amino acid residues in AA5_2 proteins compared to other characterized members

Enzyme	Organism	GenBank/JGI mycocosm Accession	Active Site Amino Acids							Distal Amino Acids	Modularity	Phylogeny Subgroup
			Radical Stabilization	Substrate Recognition/Active Site Cavity Shape						Catalytic Efficiency		
*Fgr*GalOx[a]	*Fusarium graminearum*	AAO95371	W290	F194	Q326	Y329	R330	Q406	P463	C383	CBM 32-CAT	15
*Cgr*AlcOx[b]	*Colletorichum graminicola*	EFQ30446	**F**	**W**	**G**	**F**	**M**	**T**	**L**	C	CAT	26
*Cgr*AAO[c]	*Colletorichum graminicola*	EFQ27661	**Y**	F	**E**	**W**	R	**T**	**V**	C	PAN 1-CAT	29
*Fgr*AAO[d]	*Fusarium graminearum*	XP_011322138	W	F	**E**	Y	**K**	Q	P	**N**	CBM 32-CAT	14
*Exe*GalOx	*Exophiala xenobiotica*	KIW55415	W	F	Q	**F**	R	Q	P	C	CBM-CBM 32-CAT	19
*Mre*GalOx	*Mytilinidion resinicola*	XP_033570565	W	F	Q	**F**	R	Q	P	**N**	CBM-CBM 32-CAT	3
*Fox*GalOxB	*Fusarium oxysporum*	FOTG_04629	W	**M**	Q	**F**	R	Q	P	C	UNK-CBM 32-CAT	16
*Pfe*GalOx	*Penicillium fellutanum*	382062	W	**Y**	Q	Y	R	Q	P	**S**	CBM 32-CAT	8
*Uma*RafOx	*Ustilago maydis*	XP_011389156	**Y**	F	**A**	**W**	R	**S**	**G**	C	UNK-CAT	30
*Phu*RafOx	*Pseudozyma hubeiensis*	XP_012186969.1	**Y**	F	**A**	**W**	R	**S**	**G**	C	UNK-CAT	30
*Afl*AlcOx	*Aspergillus flavus*	KAF7627372	W	**Y**	**L**	Y	**H**	**E**	P	**S**	UNK-CBM 32-CAT	7
*Pru*AA5_2A (*Pru*AlcOx)	*Penicillium rubens*	CAP96757	W	**Y**	**D**	Y	R	**E**	P	**S**	CBM 32-CAT	8
*Fox*AlcOx	*Fusarium oxysporum*	FOPG_18201	W	F	**D**	**S**	**K**	**A**	**Q**	C	CBM 32-CAT	14
*Por*AlcOx	*Pyricularia oryzae*	XP_003719369	**F**	F	**G**	**L**	**Y**	**T**	**L**	C	WSC-CAT	26
*Cgl*AlcOx	*Colletorichum gloeosporioides*	1901294	**F**	**W**	**L**	**F**	**M**	**T**	**L**	C	CAT	26
*Asy*AlcOx	*Aspergillus sydowii*	XP_040706357	**F**	**Y**	**H**	**D**	R	**V**	P	C	UNK-CBM 32-CAT	6
*Sto*AA5	*Stogonospora sp*	OAK97814	W	**Y**	**E**	**F**	R	**D**	**G**	C	CAT	28
*Cca*AA5	*Corynespora cassiicola*	PSN67470	W	**A**	**A**	**N**	**E**	**H**	**G**	C	CAT	29

Non-conserved amino acids in relation to *Fgr*GalOx are bolded. Fungal species: *Fgr Fusarium graminearum*, *Cgr Colletotrichum graminicola*, *Exe Exophiala xenobiotica*, *Mre Mytilinidion resinicola*, *Fox Fusarium oxysporum*, *Afl Aspergillus flavus*, *Pru Penicillium rubens*, *Pfe Penicillium fellutanum*, *Por Pyricularia oryzae*, *Cgl Colletotrichum gloesporoides* , *Uma Ustilago maydis*, *Phu Pseudozyma hubeiensis*, *Asy Aspergillus sydowii*, *Sto Stagonospora* sp, *Cca Corynespora cassiicola*. Modularity: Carbohydrate-binding domain (CBM), catalytic domain (CAT), PAN_1 (PF00024), WSC (PF01822), unknown domain (UNK)

Enzymes previously characterized in [a]ref [36, 92], [b]ref [37], [c]ref [39], [d]ref [40]

Protein production and initial biochemical characterization

cDNAs corresponding to the full-length sequence of 40 candidate enzymes, i.e., including any carbohydrate-binding modules (CBM [78]), PAN_1 domains (PFAM, PF00024), WSC domains (PFAM, PF01822), or unknown domains (UNK) in tandem with the catalytic AA5_2 module, were cloned into the pPICZα-A or pPICZα-C vectors in-frame with the *Saccharomyces cerevisiae* α-factor secretion signal and a C-terminal hexa-histidine tag. Fourteen proteins were thus produced successfully in *Pichia pastoris* X33 and purified via Immobilized Metal Affinity Chromatography (IMAC) followed by buffer exchange using size exclusion chromatography and SDS-PAGE analyses (Fig. S2). All proteins were obtained in full-length form except *Fox*GalOxB (species abbreviations were previously defined in Table 1), for which a truncated construct was purified. Furthermore, enzymatic deglycosylation indicated that *Afl*AlcOx, *Pru*AA5_2A (*Pru*AlcOx), *Exe*GalOx, and *Pfe*GalOx were N-glycosylated (Fig. S2). Typical protein yields varied between 2.2 and 65 mg L^{-1} based on the original volume of buffered complex methanol medium (Table S3). Overall, protein production levels were comparable to previous AA5_2 preparations from *P. pastoris*, e.g., *Fgr*AAO and *Fox*AAO (2.5 mg L^{-1}) [40], *Fox*GalOx (10.6 mg L^{-1}) [65], *Cgr*AlcOx (30–40 mg L^{-1}) [37], *Cgr*AAO (43 mg L^{-1}) [39], and the wild-type and M_1 variants of *Fgr*GalOx (120 mg L^{-1} and 110 mg L^{-1}, respectively [79]).

The fourteen successfully produced recombinant proteins were initially screened for activity using three compounds representing efficient substrates of previously characterized AA5_2 members, viz., galactose and raffinose for galactose 6-oxidases and benzyl alcohol for general alcohol oxidases (Table S4). As expected, a range of specificities was observed, with some enzymes clearly displaying higher specific activity on benzyl alcohol (*Afl*AlcOx and *Cgl*AlcOx) or galactosyl moieties (*Fox*GalOxB, *Mre*GalOx, and *Exe*GalOx), while for others this preference was equivocal (*Pfe*GalOx and *Pru*AA5_2A (*Pru*AlcOx). Notably, several targets had relatively low specific activities on all of the three substrates tested: *Uma*RafOx, *Phu*RafOx, *Cca*AA5, *Asy*AlcOx, *Fox*AlcOx, *Por*AlcOx, and *Sto*AA5. *P. pastoris* constructs of *Sto*AA5 and *Cca*AA5 produced soluble protein but the specific activities of these enzyme were not consistent between productions; hence, no further work was conducted on these two homologs.

Based on the initial activity screen results, either galactose or benzyl alcohol was chosen as the substrate for the determination of the pH-rate profile and temperature stability for each target. Exceptionally, glycerol was used as substrate for *Uma*RafOx and *Phu*RafOx following further substrate screening (specific activities > 3.0 μmol min^{-1} mg^{-1}) since these enzymes displayed very low specific activities on the three initial substrates (< 0.25 μmol min^{-1} mg^{-1}). All recombinant enzymes were active between pH 6.0 and 8.5 (Table 2) and most exhibited bell-shaped pH-rate profiles with optima between 7.0 and 8.5 in sodium phosphate buffer (Fig. S5), akin to other characterized AA5_2 enzymes [37, 39, 64, 65, 80]. Distinctly, *Mre*GalOx and *Exe*GalOx had optimum values at pH 6.0 and 6.5, respectively, while *Uma*RafOx and *Phu*RafOx were most active in glycine–NaOH buffer at pH 8.5.

Most AA5_2 enzymes were stable at 30 °C, similar to some previously characterized members [37, 39]. Three enzymes (*Fox*GalOxB, *Afl*AlcOx and *Pru*AA5_2A (*Pru*AlcOx)) were stable between 35 and 40 °C, similar to *Fox*GalOx (40 °C) [65], and three enzymes (*Exe*GalOx, *Mre*GalOx and *Fox*AlcOx) exhibited higher thermostabilities than previously characterized CROs (45 °C–55 °C) (Table 2 and Fig. S6). Cumulatively, these results are consistent with the mesophilic nature of their natural hosts. Due to instrument limitations, the substrate screening was performed at ambient temperature, while subsequent Michaelis–Menten kinetic assays were performed at temperatures that balanced optimal enzyme activity with short-term stability.

Extended substrate screening and Michaelis–Menten kinetics

After establishing preferred assay parameters for the 12 demonstrably active AA5_2 targets, these enzymes were screened in parallel, using a multi-well plate assay, against a broader panel of primary alcohol-containing substrates comprising carbohydrates, alkanols, and aryl alcohols with relevance to biomass utilization, pharmaceutical preparation, or biomaterial synthesis (Fig. 2). Based upon the outcome of this extended screen, key substrates were selected based on specific activity values for detailed Michaelis–Menten kinetic analysis (Table 2 and Fig. S7–S18). Taken together, these assays enabled us to group enzymes by their predominant activities, which are discussed below in the context of their molecular phylogeny and SSN clustering.

Galactose 6-oxidases

Enzymes in this group predominantly possess the canonical galactose 6-oxidase activity (EC 1.1.3.9) that first defined the CRO family [81–83]. As such, they have minimal to no activity on other polyols, diols, and other non-carbohydrate primary alcohols. The activity profile of

Table 2 Initial rate kinetics of active AA5_2 enzymes*

Enzyme	Substrate	K_M (mM)	k_{cat} (s^{-1})	k_{cat}/K_M ($M^{-1}.s^{-1}$)	Condition
*Exe*GalOx	Galactose	25 ± 4.0	130 ± 3.7	(5.2 ± 0.8) × 10^3	pH 6.0, 49 °C
	Melibiose	25 ± 0.6	37 ± 0.2	(1.5 ± 0.03) × 10^3	
*Mre*GalOx	Galactose	64 ± 4.8	32 ± 0.7	(5.0 ± 0.4) × 10^2	pH 6.0, 55 °C
	Melibiose	n.d.§	n.d.§	(1.8 ± 0.8) × 10^2	
*Fox*GalOxB	Galactose	24 ± 1.3	81 ± 1.0	(3.4 ± 0.2) × 10^3	pH 8.0, 39 °C
	Melibiose	n.d.§	n.d.§	(5.9 ± 1.7) × 10^3	
*Pfe*GalOx	Glycerol	69 ± 1.6	140 ± 1.1	(2.0 ± 0.1) × 10^3	pH 8.5, 30 °C
	Galactose	28 ± 6.7	140 ± 4.5	(5.0 ± 1.2) × 10^3	
*Uma*RafOx	Glycerol	2900 ± 720	130 ± 24	45 ± 14	pH 8.5, 30 °C
	Raffinose	450 ± 94	130 ± 15	290 ± 69	
*Phu*RafOx	Glycerol	2900 ± 390	56 ± 3.8	19 ± 2.9	pH 8.5, 30 °C
	Raffinose	410 ± 33	8.8 ± 0.5	21 ± 2.1	
*Afl*AlcOx	Benzyl Alcohol	19 ± 1.9	410 ± 11	(2.1 ± 0.2) × 10^4	pH 8.5, 39 °C
	HMF	5.0 ± 1.3	190 ± 20	(3.8 ± 1.1) × 10^4	
	Galactose	980 ± 61	400 ± 10	(4.1 ± 0.3) × 10^2	
*Pru*AA5_2A (*Pru*AlcOx)	Glycerol	34 ± 1.7	170 ± 3.0	(4.9 ± 0.3) × 10^3	pH 7.5, 35 °C
	Galactose	110 ± 18	220 ± 8.6	(2.0 ± 0.3) × 10^3	
	Benzyl Alcohol	9.2 ± 1.8	110 ± 5.0	(1.2 ± 0.2) × 10^4	
*Fox*AlcOx	Benzyl Alcohol	230 ± 70	24 ± 4.5	100 ± 37	pH 8.5, 45 °C
	Galactose	2000 ± 650	8.3 ± 1.7	4.1 ± 1.6	
*Por*AlcOx	Benzyl Alcohol	1.3 ± 0.10	8.6 ± 0.15	(6.6 ± 0.5) × 10^3	pH 7.5, 30 °C
	Butanol	4.6 ± 0.30	7.9 ± 0.09	(1.7 ± 0.1) × 10^3	
	Glycerol	57 ± 8.1	8.5 ± 0.32	(1.5 ± 0.2) × 10^2	
	1,4-Butanediol	4.3 ± 0.56	9.5 ± 0.51	(2.2 ± 0.3) × 10^3	
*Cgl*AlcOx	Benzyl Alcohol	3.6 ± 0.8	350 ± 20	(9.7 ± 2.2) × 10^4	pH 8.0, 30 °C
	HMF	0.09 ± 0.01	240 ± 16	(2.7 ± 0.3) × 10^6	
	1,4-Butanediol	3.9 ± 0.4	330 ± 13	(8.5 ± 0.9) × 10^4	
*Asy*AlcOx	Benzyl Alcohol	79 ± 22	17 ± 1.8	(2.2 ± 0.6) × 10^2	pH 8.0, 30 °C
	Glycerol	700 ± 80	38 ± 2.0	54 ± 6.8	

*Error bars represent the standard deviation from the mean values

§ Individual K_M and k_{cat} values not determinable; k_{cat}/K_M values obtained from slope of linear v_0 versus [S] plots (see panels B in Figs. S7–S18)

these enzymes is comparable to the archetype, *Fgr*GalOx [59, 84].

*Exe*GalOx

*Exe*GalOx is located alone within clade 19 in the phylogenetic tree and it possesses low sequence similarity to its closest homologs *Fox*GalOxB and the archetypal *Fgr*GalOx (40% and 47%, respectively) (Fig. 1 and Table S2). *Exe*GalOx displayed moderate specific activity on galactose and showed lower but equivalent specific activities on raffinose and melibiose; hence, we categorized this enzyme as a galactose oxidase (EC 1.1.3.9) (Table S5 and Fig. S7). Compared to *Fgr*GalOx, *Exe*GalOx had a threefold lower catalytic efficiency on galactose due to a lower k_{cat} even though its K_M was fourfold lower (Tables 2, S11, and Fig. S7). In addition, *Exe*GalOx had a threefold lower catalytic efficiency on melibiose compared to galactose, which reflects a lower turnover rate since the K_M for both substrates is the same (Table 2 and Fig. S7).

*Mre*GalOx

*Mre*GalOx also is located alone in clade 3 and shares low sequence identity with the closest neighboring homologs: 35% vs. *Asy*AlcOx and 39% vs. *Afl*AlcOx (Fig. 1 and Table S2). *Mre*GalOx exhibited low production yields and lower activity compared to other enzymes presented in this study. No activity above the limit of detection of our assay (9×10^{-4} µmol min^{-1} mg^{-1} using 0.85 µM of purified enzyme) was observed with many substrates. Nonetheless, *Mre*GalOx demonstrated low specific activity on galactose and comparable specific activities on raffinose and melibiose; thus, we designated this enzyme as a galactose oxidase

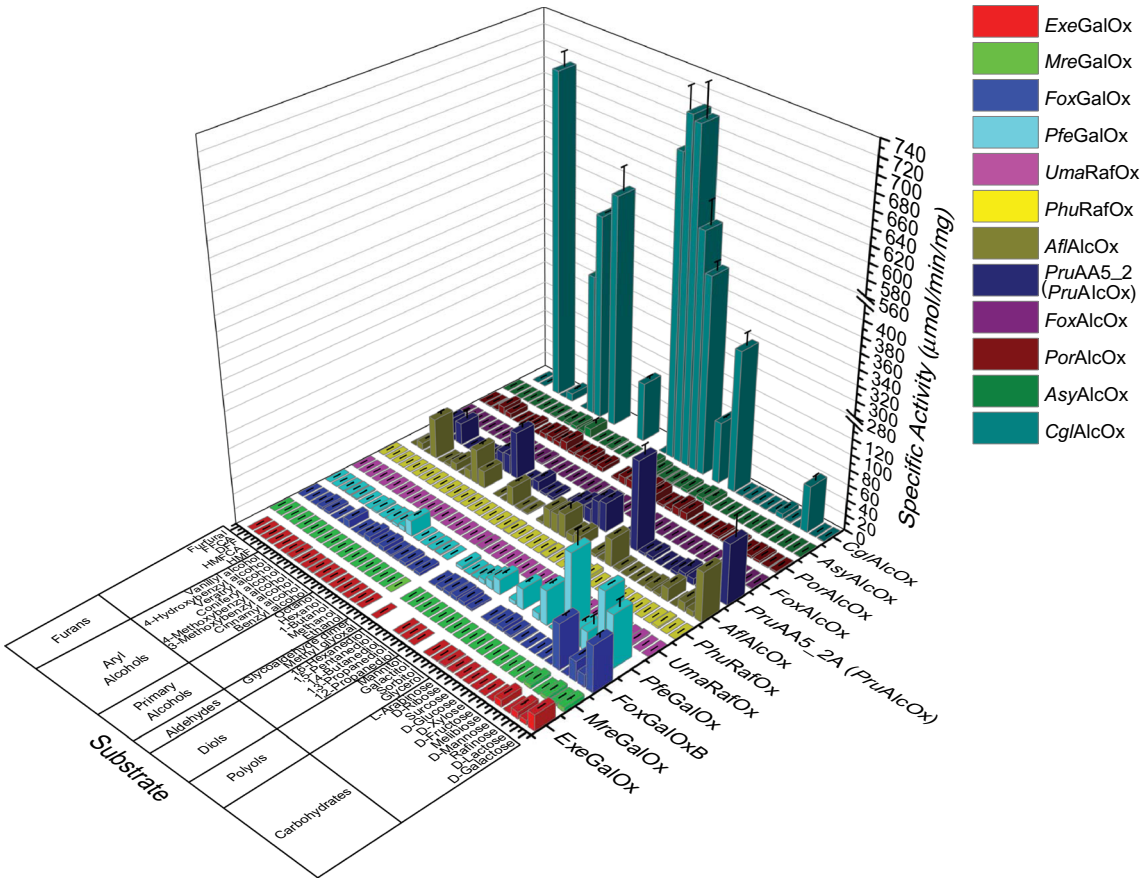

Fig. 2 Extended activity screening of AA5_2 enzymes. Measurements were performed in triplicate at room temperature in 100 mM buffer, using the HRP/ABTS assay. Activities were monitored using 300 mM for carbohydrates, polyols, diols, and primary alcohols, 30 mM for benzyl alcohol and galactitol, 2.5 mM for aldehydes, aryl alcohols, and furans. Reactions were started with the addition of 30 pmol–0.26 nmol of purified enzyme

(EC 1.1.3.9) (Fig. S8 and Table S5). Compared to *Fgr*GalOx, *Mre*GalOx had a 20-fold lower catalytic efficiency on galactose (Tables 2, S11, and Fig. S8). Comparing its activity on melibiose versus galactose, *Mre*GalOx had a threefold higher catalytic efficiency on melibiose; however, K_M and k_{cat} parameters could not be reliably determined due to apparent substrate inhibition (Table 2 and Fig. S8).

*Fox*GalOxB

*Fox*GalOxB is located alone in clade 16 next to clade 15, which contains the archetypal *Fgr*GalOx and other characterized galactose 6-oxidases (Fig. 1). Only 40% identity is shared between *Fox*GalOxB and *Fgr*GalOx, despite the close phylogenetic association (Table S2). The full substrate profile of *Fox*GalOxB led us to designate it as a galactose oxidase (EC 1.1.3.9). Since a galactose oxidase has already been characterized in *Fusarium oxysporum* [65], we have named this homolog *Fox*GalOxB [85]. *Fox*GalOxB showed high specific activity on galactose and melibiose, followed by raffinose and then lactose, whereas low specific activity was observed on polyols, diols, and primary and aryl alcohols (Fig. S9 and Table S6). In addition, *Fox*GalOxB showed low specific activity on both HMF and HMFCA (3.3 µmol min^{-1} mg^{-1}), low specific activity on DFF, and no activity on FFCA (Fig. S9 and Table S6). Compared to the archetypal *Fgr*GalOx, *Fox*GalOxB had a threefold lower catalytic efficiency on galactose (Tables 2, S11, and Fig. S9). Substrate inhibition was also observed on melibiose with *Fox*GalOxB and an overall twofold decrease in catalytic efficiency compared to galactose was found (Table 2 and Fig. S9).

*Pfe*GalOx

*Pfe*GalOx is located in clade 8, which also contains *Pru*AA5_2A (*Pru*AlcOx) (56% identity) and is located next to the clade containing *Afl*AlcOx (51% identity) (Fig. 1 and Table S2). Analogous to *Fox*GalOxB, *Pfe*GalOx displayed high specific activity on galactose; however,

other galactosylated carbohydrates showed moderate specific activity, with its highest activity observed on raffinose, followed by lactose, and lastly melibiose (Fig. S10 and Table S6). Interestingly, *Pfe*GalOx also showed prominent specific activity on xylose (Fig. S11 and Table S6), which is a novel activity among CROs. Furthermore, *Pfe*GalOx displayed high specific activity on glycerol, and moderate activities on benzyl alcohol, butanol, and 1,2-propanediol/1,3-propanediol, yet low activity on other primary alcohols (Fig. S10 and Table S6). Considering the full substrate profile of *Pfe*GalOx, we have classified this enzyme as a galactose oxidase (EC 1.1.3.9). *Pfe*GalOx had a twofold lower catalytic efficiency on galactose than *Fgr*GalOx [72] attributable to both an eightfold decrease in k_{cat} and a fourfold decrease in K_M (Tables 2, S11, and Fig. S10). Furthermore, *Pfe*GalOx showed a twofold higher catalytic efficiency on glycerol than *Cgr*AlcOx [37]; however, it had a 2.5-fold higher catalytic efficiency on galactose compared to glycerol (Tables 2, S12, and Fig. S10).

Raffinose oxidases

Raffinose oxidases (EC 1.1.3.-), from the perspective of specificity, can be considered as a subclass of the galactose 6-oxidases, because these enzymes oxidize the hydroxyl group located on the carbon 6 of the galactosyl residue of this trisaccharide. Nonetheless, these enzymes exhibit a distinct specificity for raffinose over galactose and other galactosides, as has been demonstrated for *Cgr*RafOx [62]. These enzymes are also comparably proficient at oxidizing glycerol, some diols, and glycolaldehyde dimer.

*Uma*RafOx

*Uma*RafOx is located in a distinct clade (clade 30; Fig. 1 and Table S2), which also contains *Phu*RafOx (81% identity) and the previously characterized *Cgr*RafOx (43% identity). *Uma*RafOx showed low specific activity on glycerol, compared to other enzymes in the present study. Nonetheless, this polyol is the substrate for which the highest specific activity was observed for this enzyme (Fig. S11 and Table S7). *Uma*RafOx showed an overall low specific activity on carbohydrates; however, the substrate for which *Uma*RafOx had the second highest specific activity was raffinose (Fig. S12 and Table S7). *Uma*RafOx also displayed a similar specific activity to raffinose on glycolaldehyde dimer; however, no activity on methyl glyoxal was observed (Fig. S12 and Table S7). *Uma*RafOx had a 20-fold lower catalytic efficiency on glycerol compared to *Cgr*AlcOx [37], and a 15-fold higher catalytic efficiency on glycerol compared to *Cgr*RafOx (Tables 2 and S12). The catalytic efficiency of *Uma*RafOx on raffinose is sixfold higher than *Cgr*RafOx [62] (Table 2). Based on these kinetic results, we designated *Uma*RafOx as a raffinose oxidase (EC 1.1.3.-).

*Phu*RafOx

*Phu*RafOx has a substrate profile similar to *Uma*RafOx, displaying high activity on glycerol followed by raffinose (Fig. S12 and Table S7). *Phu*RafOx also showed low equivalent specific activities on glycolaldehyde dimer and 1,3-propanediol (Fig. S12 and Table S7). *Phu*RafOx had a 50-fold lower catalytic efficiency on glycerol compared to *Cgr*AlcOx [37], and a sixfold higher catalytic efficiency on glycerol compared to *Cgr*RafOx (Tables 2 and S12). The catalytic efficiency of *Phu*RafOx on raffinose is twofold lower than *Cgr*RafOx; however, considering the fully distinct substrate profile we classified *Phu*RafOx as a raffinose oxidase (EC 1.1.3.-).

Broad-spectrum alcohol oxidases

Enzymes in this group exhibit a broad catalytic range, i.e., a lack of selectivity, for carbohydrates, including galactose and galactosides (EC 1.1.3.9), linear alcohols, including diols and polyols (EC 1.1.3.13), as well as diverse aryl alcohols, including benzyl alcohols and furan derivatives (EC 1.1.3.7 and EC 1.1.3.47). At the same time, these enzymes demonstrate distinct substrate preferences within these compound classes. The activity profiles of these enzymes are reminiscent of *Fgr*AAO[40] and *Cgr*AAO[39].

*Afl*AlcOx

*Afl*AlcOx is located alone in clade 7 in the phylogenetic tree and shares moderate sequence identity with its closest homologs *Pfe*GalOx and *Pru*AA5_2A (*Pru*AlcOx) (51% and 48%, respectively) (Fig. 1 and Table S2). *Afl*AlcOx showed high specific activity on benzyl alcohol and moderate specific activities on galactose, glycerol, diols, butanol, HMF, and other aryl alcohols (Fig. S13 and Table S8). Due to this broad range of activities, we have designated *Afl*AlcOx as a general alcohol oxidase (EC 1.1.3.13 and EC 1.1.3.7). *Afl*AlcOx showed a sevenfold lower catalytic efficiency compared to *Cgr*AlcOx on benzyl alcohol (Table S12) and showed a higher catalytic efficiency on HMF than *Cgr*AAO, bacterial HMFO (a Glucose-Methanol-Choline (GMC) superfamily oxidoreductase) and *Fgr*AAO (twofold, fivefold, and 20-fold, respectively) (Table S13). Even though *Afl*AlcOx displayed prominent specific activity on galactose, its catalytic efficiency on benzyl alcohol was 50-fold higher than

on galactose (Table 2 and Fig. S13). Furthermore, *Afl*AlcOx had a 25-fold lower catalytic efficiency on galactose than the archetypal *Fgr*GalOx, due to a tenfold increase in K_M and a threefold decrease in k_{cat} compared to *Fgr*GalOx (Table S11).

*Pru*AA5_2A (*Pru*AlcOx)

*Pru*AA5_2A (*Pru*AlcOx) is located in the same clade as *Pfe*GalOx (56% identity) and shares 48% identity with *Afl*AlcOx located in the neighboring clade (Fig. 1 and Table S2). *Pru*AA5_2A (*Pru*AlcOx) displayed high specific activity on glycerol, moderate activities on 1,2-propanediol, and 1,3-propanediol and showed decreased specific activities with increasing chain length on other diols (Fig. S14 and Table S8). *Pru*AA5_2A (*Pru*AlcOx) also showed high specific activity on galactose, but low activities were observed for other carbohydrates. Furthermore, *Pru*AA5_2A (*Pru*AlcOx) showed high specific activity on benzyl alcohol and moderate specific activity on HMF with lower activity observed on HMFCA, very low activity on DFF, and no activity on FFCA (Fig. S14 and Table S8). Based on this wide substrate scope, we have classified *Pru*AA5_2A (*Pru*AlcOx) as a general alcohol oxidase (EC 1.1.3.13 and EC 1.1.3.7). *Pru*AA5_2A (*Pru*AlcOx) displayed catalytic efficiencies fivefold higher on glycerol and tenfold lower on benzyl alcohol than *Cgr*AlcOx [37] (Table S12). Despite *Pru*AA5_2A (*Pru*AlcOx) possessing a high specific activity on galactose, similar to *Afl*AlcOx, the catalytic efficiency of *Pru*AA5_2A (*Pru*AlcOx) on benzyl alcohol was 25-fold higher than that on galactose (Table S11). *Pru*AA5_2A (*Pru*AlcOx) has a similar K_M value on galactose and shows a fivefold lower turnover rate compared to *Fgr*GalOx (Table S11).

During the course of the present study *Pru*AA5_2A (*Pru*AlcOx) was characterized as exhibiting an activity profile combining those of AA5_1 and AA5_2 members [61]. Here, we observed generally higher activities on all tested substrates and a different specificity profile. In our hands, *Pru*AA5_2A (*Pru*AlcOx) possessed a higher specific activity on galactose rather than raffinose [61] (ninefold) and the highest specific activity was observed on glycerol rather than the glycolaldehyde dimer [61] (twofold) at the equivalent concentrations as the previous study. Furthermore, our enzyme exhibited substantial specific activity on benzyl alcohol (84 µmol min^{-1} mg^{-1} at 30 mM), while the previous study did not observe any activity on this substrate at 300 mM [61]. The reasons for these discrepancies are unclear, but we note that *P. pastoris* SMD1168H and fed-batch production were used previously vs. *P. pastoris* X33 shake-flask production here.

*Fox*AlcOx

*Fox*AlcOx is located in the same clade as the recently characterized *Fgr*AAO and *Fox*AAO (clade 14) (67% identity) (Fig. 1 and Table S2). This clade is located beside the classical galactose oxidases, and *Fox*AlcOx shares 58% identity with *Fgr*GalOx. *Fox*AlcOx has generally low specific activities on all substrates tested and displayed the lowest specific activity out of all the enzymes presented in this study (Fig. S15 and Table S9). *Fox*AlcOx showed the highest specific activity on benzyl alcohol, while the second highest specific activities were observed on galactose and the aldehyde compounds, i.e., methyl glyoxal and glycolaldehyde dimer (Fig. S15 and Table S9). The catalytic efficiency of *Fox*AlcOx on benzyl alcohol is 1400-fold lower than *Cgr*AlcOx [37] and fourfold lower than *Fgr*GalOx[86] (Table S12). Due to this broad substrate range, which includes carbohydrates, aryl alcohols, and aldehydes (which likely react with the enzyme in their hydrated forms [34, 35]), we have classified *Fox*AlcOx as a general alcohol oxidase (EC 1.1.3.13 and EC 1.3.3.7). Since the second highest specific activity for *Fox*AlcOx was observed on galactose, Michaelis–Menten kinetics were performed for this substrate and showed that *Fox*AlcOx displayed a 2500-fold lower catalytic efficiency on galactose than *Fgr*GalOx (Table S11).

*Por*AlcOx

*Por*AlcOx is located in the same distinct clade as *Cgl*AlcOx (57% identity), *Cgr*AlcOx (55% identity), and other previously characterized AlcOxs (clade 26) (Fig. 1 and Table S2). Similar to *Mre*GalOx, *Por*AlcOx was produced with low yields (Table S3). Nevertheless, comparable moderate specific activities were measured on polyols, diols, primary alcohols, and aryl alcohols with notable activity on benzyl alcohol and HMFCA (Fig. S16 and Table S10). In contrast to *Afl*AlcOx and *Pru*AA5_2A *(Pru*AlcOx), *Por*AlcOx showed higher activity on HMFCA versus HMF while also displaying low activities on DFF and FFCA (Fig. S16 and Table S10). The broad substrate profile of *Por*AlcOx is indicative of a general alcohol oxidase (EC 1.1.3.13) (Fig. S16 and Table S10). *Por*AlcOx had lower catalytic efficiencies compared to *Cgr*AlcOx [37], i.e., k_{cat}/K_M values were 20-fold less on benzyl alcohol, 40-fold less on 1,4-butanediol, 80-fold less on butanol, and sixfold less on glycerol (Table 2 and S12). During the course of our study, *Por*AlcOx was characterized using ethanol, butanol, 1,3-butanediol, and glycerol as substrates. Although we did not obtain kinetic parameters on all of the aforementioned substrates, our catalytic efficiencies on butanol and glycerol are comparable to the previously reported values [38].

Non-carbohydrate alcohol oxidases

Enzymes in this group clearly appear to reject mono-, di-, and trisaccharides, notably including galactose and raffinose, in favor of alkanols and aryl alcohols (EC 1.1.3.7 and EC 1.1.3.47). At the same time, these enzymes are generally proficient on linear diols and polyols. The activity profiles of these enzymes are reminiscent of *Cgr*AlcOx and *Cgl*AlcOx [37].

*Cgl*AlcOx

*Cgl*AlcOx is located in the same clade as *Por*AlcOx, *Cgr*AlcOx, *Cgl*AlcOx, and *Chi*AlcOx (clade 26) (Fig. 1). Furthermore, it shares 79% identity with *Cgr*AlcOx (Table S2) and 99% identity with *Cgl*AlcOx from *C. gloesporoides-14*/*Colletotrichum fructicola Nara gc5*. The *Cgl*AlcOx characterized in this study is from *C. gloesporoides-23* and contains a single point mutation compared to the previously characterized *Cgl*AlcOx [37]. *Cgl*AlcOx displays higher activity under acidic conditions, lower thermostability and the same catalytic efficiency on benzyl alcohol (Table 2, and Figs. S5, S6, S17) compared to its ortholog. *Cgl*AlcOx showed equally high specific activities on all diols, glycerol, primary alcohols, benzyl alcohols, and substituted aryl alcohols; hence, we characterized this enzyme as a general alcohol oxidase (EC 1.1.3.7 and EC 1.1.3.13) (Fig. S17 and Table S10). *Cgl*AlcOx had catalytic efficiencies comparable to *Cgr*AlcOx [37] on benzyl alcohol and 1,4-butanediol and that are 50-fold and 40-fold higher, respectively, compared to *Cgr*AAO [39] (Tables 2 and S12). Moreover, *Cgl*AlcOx displayed high specific activity on HMF while showing almost no activity on DFF and FFCA (Fig. S17 and Table S10). *Cgl*AlcOx had the highest reported catalytic efficiency to date on HMF with a 140-fold higher k_{cat}/K_M value than *Cgr*AAO [39] and a 380-fold higher k_{cat}/K_M value than the bacterial HMFO [87] (a GMC superfamily oxidoreductase) (Table S13). As such, *Cgl*AlcOx may also be classified as an HMF oxidase (EC 1.1.3.47).

*Asy*AlcOx

*Asy*AlcOx is located alone in clade 6 and shares only 45% identity with *Afl*AlcOx in the neighboring clade (Fig. 1 and Table S2). *Asy*AlcOx possessed moderate specific activities on aryl alcohols and diols, but notable specific activity on benzyl alcohol; thus, we designated this enzyme as a general alcohol oxidase (EC 1.1.3.13 and EC 1.3.3.7). *Asy*AlcOx showed low activity on diols while displaying enhanced specific activity with increased carbon chain length, culminating with 1,6-hexanediol (Fig. S18 and Table S9). Michaelis–Menten kinetics indicated that *Asy*AlcOx had over 600-fold and 17-fold lower catalytic efficiencies on benzyl alcohol and glycerol, respectively, than *Cgr*AlcOx [37] (Tables 2, S11 and Fig. S18).

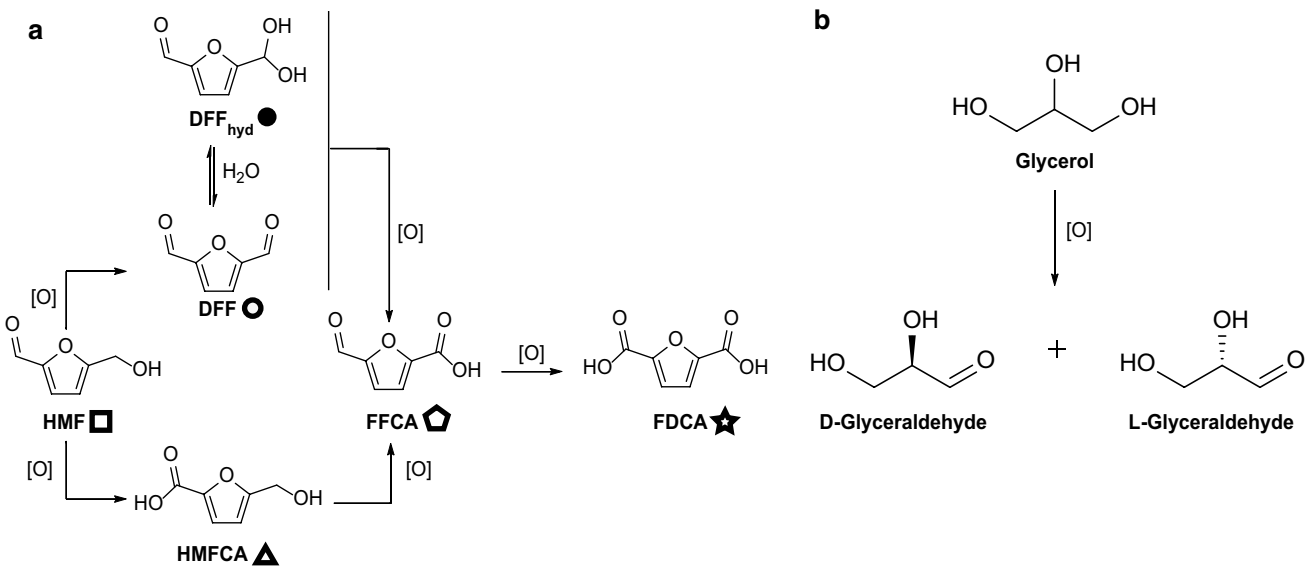

Fig. 3 Oxidation pathways of HMF and Glycerol. **a** HMF oxidation pathway. The symbols next to each compound are used to denote the corresponding peaks in the NMR spectra comprising Figs. S19–S23. **b** Glycerol oxidation pathway showing L- and D-glyceraldehyde. [O] represents a generic oxidant

Application to bioproduct conversion

CROs from AA5 are finding increasing applications in the conversion of small molecules to valuable chemical intermediates [46, 47, 50, 55, 56, 59, 88, 89]. Among these, HMF from the thermochemical breakdown of plant biomass [57, 58] and glycerol, a by-product of the biodiesel industry [90], are of particular interest. On one hand, HMF can be converted into the bi-functional polymer precursors DFF and FDCA by controlled oxidation (Fig. 3a) [57, 58]. On the other hand, glycerol is an exemplar prochiral compound and its valorization through desymmetrization has garnered significant interest (Fig. 3b). Relatedly, an evolved variant of *Fgr*GalOx was used for an essential desymmetrization of a key 2-ethynyl-glycerol intermediate in the biocatalytic cascade synthesis of the antiviral drug islatravir [55].

HMF

Enzymes with specific activities above 3 μmol min^{-1} mg^{-1} on any furan substrate were incubated with either 10 mM HMF, HMFCA, DFF, or FFCA, followed by direct quantitation of the product(s) by ^{1}H NMR (Table 3). Previous work has shown that *Cgr*AAO oxidized HMF to DFF, while *Fgr*AAO produced a mixture of DFF and FFCA as the terminal products of HMF oxidation [39, 40].

*Cgl*AlcOx showed 100% conversion of HMF to a 91:9 mixture of FFCA and FDCA, respectively (Table 3 and Fig. S19). Based on experiments with the HMF oxidation pathway intermediates HMFCA and DFF, *Cgl*AlcOx is able to oxidize both furans efficiently with the major product consisting of FFCA with some FDCA observed (Table 3 and Fig. S19). *Por*AlcOx, which belongs to the same cluster as *Cgl*AlcOx, showed incomplete conversion of 10 mM HMF producing predominantly DFF with 2% FFCA observed (Table 3 and Fig. S20). Interestingly, *Por*AlcOx showed full conversion of HMFCA and DFF to mostly FFCA, and partial conversion to FDCA was also observed (Table 3 and Fig. S20).

*Pru*AA5_2A (*Pru*AlcOx) oxidized 100% of 10 mM HMF to DFF (including its hydrated form) and FFCA(Table 3 and Fig. S21). *Afl*AlcOx showed similar conversion percentages to *Pru*AA5_2A (*Pru*AlcOx) for HMF, HMFCA, and DFF (Table 3 and Fig. S22). However, no conversion was observed with FFCA for *Afl*AlcOx. *Fox*GalOxB displayed low percent conversion of HMF and had a similar product profile to *Pru*AA5_2A (*Pru*AlcOx) (Table 3 and Fig. S23).

In previous work, the aryl oxidase *Fgr*AAO, was shown to produce similar ratios of products during overnight incubations with furan-containing substrates compared to *Pru*AA5_2A (*Pru*AlcOx), *Afl*AlcOx, and *Fox*GalOxB [40]. It was noted for *Fgr*AAO, and other CRO enzymes, that perhaps the low degree of hydration of FFCA compared to DFF limits further conversion [87]. In contrast, the increased production of FDCA observed for both *Cgl*AlcOx and *Por*AlcOx may be caused by their active-site architecture being able to accommodate the aldehyde form (or its hydrate) of

Table 4 Stereochemical outcome of glycerol oxidation by AA5 CROs

AA5 CRO	Product	
	L-glyceraldehyde hydrazone (%)	D-glyceraldehyde hydrazone (%)
*Fgr*GalOx[a]	96	4
*Cgr*AlcOx[a]	10	90
*Fox*GalOxB	79	21
*Pfe*GalOx	71	29
*Uma*RafOx	84	16
*Phu*RafOx	82	18
*Afl*AlcOx	88	12
*Pru*AA5_2A (*Pru*AlcOx)	96	4
*Cgl*AlcOx	3	97
*Por*AlcOx	11	89
AsvAlcOx	77	23

[a]Enzymes previously characterized in ref [40]

Table 3 Percent conversions of HMF, HMFCA, DFF, and FFCA by *Pru*AA5_2A (*Pru*AlcOx), *Afl*AlcOx, *Cgl*AlcOx, *Por*AlcOx, and *Fox*GalOxB

AA5 CRO	Substrate			
	HMF	HMFCA	DFF	FFCA
*Fox*GalOxB	DFF (29%), FFCA (4%)	FFCA (17%)	FFCA (12%)	FDCA (7%)
*Afl*AlcOx	DFF (52%), FFCA (48%)	FFCA (100%)	FFCA (40%)	0%
*Pru*AA5_2A (*Pru*AlcOx)	DFF (52%), FFCA (48%)	FFCA (100%)	FFCA (38%)	FDCA (5%)
*Cgl*AlcOx	FFCA (91%), FDCA (9%)	FFCA (92%), FDCA (8%)	FFCA (87%), FDCA (13%)	FDCA (24%)
*Por*AlcOx	DFF (49%), FFCA (2%)	FFCA (83%), FDCA (17%)	FFCA (72%), FDCA (28%)	FDCA (49%)

FFCA, which results in higher percent conversions to FDCA compared to other CROs.

Glycerol

It has been previously reported that the wild-type *Fgr*GalOx and *Fgr*AAO oxidize glycerol stereoselectively to L-glyceraldehyde, while *Cgr*AlcOx produces the natural D-glyceraldehyde isomer [40, 91]. To explore the stereoselectivity of CROs in the present study, those with specific activities toward glycerol greater than 3 μmol min^{-1} mg^{-1} were incubated with 0.54 M glycerol for 24 h, followed by chiral HPLC analysis of the resulting 2,4-dinitrophenyl glyceraldehyde-hydrazones (Table 4 and Fig. S24).

*Cgl*AlcOx and *Por*AlcOx showed a preference for producing D-glyceraldehyde with an *er* of 3:97 and 11:89 (L-:D-), respectively. This may be expected, since both share higher identity with *Cgr*AlcOx (79% and 55%, respectively) than with *Fgr*GalOx (38% and 34%) (Table S2). On the other hand, all of the other enzymes tested for the stereoselective oxidation of glycerol showed a strong preference for the formation of L-glyceraldehyde (Table 4 and Fig. S24). These enzymes all have higher identities to *Fgr*GalOx (52–36%) than *Cgr*AlcOx (33–23%) (Table S2), providing further evidence that the different active-site amino acid scaffolds of *Fgr*GalOx and *Cgr*AlcOx direct the stereoselective oxidation of achiral glycerol.

Discussion

Biocatalysis will play an increasingly important role in the development of a sustainable economy, and the discovery of novel enzymes, particularly oxidases, is essential to support this transition. Only recently it has been appreciated that the range of native catalytic activities found among the copper radical oxidases from Auxiliary Activity Family 5 Subfamily 2 members extends beyond the founding, classical galactose 6-oxidases [37–39]. In the present study, we have biochemically characterized twelve AA5_2 members dispersed across the AA5_2 phylogenetic tree, covering hitherto unexplored clades. These comprise four canonical galactose-6-oxidases (*Exe*GalOx, *Mre*GalOx, *Fox*GalOxB, and *Pfe*GalOx), two raffinose-specific galactosyl oxidases (*Uma*RafOx and *Phu*RafOx), four broad-spectrum alcohol oxidases (*Afl*AlcOx, *Pru*AA5_2A (*Pru*AlcOx), *Fox*AlcOx, and *Por*AlcOx), and two alcohol oxidases that notably do not target carbohydrates (*Cgl*AlcOx and *Asy*AlcOx). Mapping these activities onto the current phylogenetic landscape of AA5_2 indicated that although a number of clades demonstrate conserved substrate specificities, such as clade 15 with GalOxs, clade 30 with RafOxs, and clade 26 with AlcOxs, galactosyl versus general alcohol oxidase activity was not monophyletic. However, detailed analysis of active-site residues, supported by structural homology modeling based on *Fgr*GalOx (PDB ID 1GOF) [92] and computational docking of galactose (Figs. 4 and S25–S27), allows us to rationalize some structure–function relationships among the CROs in the absence of experimental tertiary structures of these homologs.

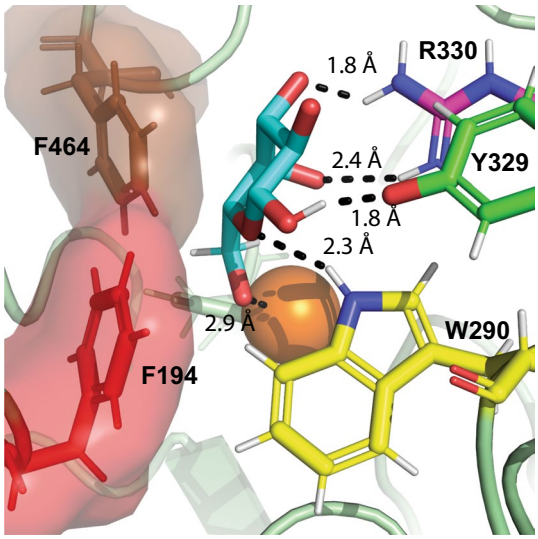

Fig. 4 Molecular docking of galactose (cyan) into the experimental tertiary structure of *Fgr*GalOx (PDB ID 1GOF) [92]. The copper atom is depicted as a dark orange sphere, while W290, Y329, R330, F494, and F194 are depicted as yellow, green, magenta, brown, and red sticks, respectively, including surface representation for F194 and F464. Ligand coordination is indicated in black

Four CROs displayed similar substrate profiles to the archetypal galactose oxidase; however, *Exe*GalOx, *Mre*GalOx, and *Fox*GalOxB have a distinct difference with a phenylalanine at the position corresponding to Y329 in *Fgr*GalOx (Table 1). Although this residue has been suggested to form a hydrogen bond with the 1-OH of galactose [77] (Fig. 4), *Exe*GalOx, *Mre*GalOx, and *Fox*GalOxB all have lower K_M values than the archetypal enzyme (Table S11), thus indicating that this tyrosine is dispensable to maintain efficient galactose binding. Computational docking suggests that other predicted hydrogen bonds to active-site arginine and tryptophan residues may be sufficient for galactose binding in these enzymes, such as observed in *Exe*GalOx (Fig. S25-B).

Consistent with this hypothesis, three broad-spectrum alcohol oxidases (*Fox*AlcOx, *Afl*AlcOx and *Pru*AA5_2A (*Pru*AlcOx)) also showed prominent activity on galactose. Of these, the enzymes with K_M values equal to, or lower than, *Fgr*GalOx on galactose retained an arginine at the corresponding position (Arg330, Tables 1 and S10). This amino acid has been speculated to make two hydrogen bonds with the 3-OH and 4-OH of galactose [69], which is supported

by docking analysis of *Fgr*GalOx and *Exe*GalOx (Figs. 4 and S26-B). However, enzymes with a lysine (*Fox*AlcOx) or a histidine (*Afl*AlcOx) at this position have higher K_M values, possibly caused by the loss of hydrogen bonding interactions. *Fox*AlcOx possesses a lysine that only forms one predicted hydrogen bond to galactose (2.7 Å) (Fig. S26-C), and the limited activity of this homolog is similar to previously studied AA5_2 members with this substitution [40, 72] (Table S11). Likewise, the longer effective distance between the histidine and galactose modeled in *Afl*AlcOx likely diminishes the potential of hydrogen bonding (Fig. S26-D). With the exception of *Cgr*AAO [39] and *Asy*AlcOx, other enzymes with no activity on galactose feature a methionine or a tyrosine residue at the position corresponding to Arg330 in *Fgr*GalOx (Table 1).

Another residue that appears to be important in determining galactose binding is F194, which together with F464 is speculated to form a hydrophobic wall in *Fgr*GalOx [69]. Our models indeed support that this wall may interact with the comparatively hydrophobic bottom face (defined by the axial H-1, H-3, and H-5) of β-galactopyranoside, as well as the exocyclic CH_2 group (Fig. 4). Enzymes with a substitution at the position corresponding to F194 in *Fgr*GalOx and demonstrable galactose oxidase activity (> 60 μmol min^{-1} mg^{-1}, viz., *Pfe*GalOx, *Afl*AlcOx, *Pru*AA5_2A (*Pru*AlcOx) with tyrosine and *Fox*GalOxB with methionine) all have lower k_{cat} values and overall lower catalytic efficiencies, despite some having lower K_M values (*Pfe*GalOx and *Pru*AA5_2A (*Pru*AlcOx) (Table S11). Modeling of *Pfe*GalOx, *Afl*AlcOx, and *Pru*AA5_2A (*Pru*AlcOx) with galactose also suggests that the corresponding tyrosine can also form a hydrophobic wall with the bridging phenylalanine. However, this tyrosine is also computed to be within hydrogen bonding distance to the ring oxygen of galactose and, consequently, may orient the 6-OH further away from the copper center compared to *Fgr*GalOx, thereby attenuating activity (Fig. S27-B–D).

Confoundingly, *Fox*GalOxB, has a methionine in the position corresponding to position 194 in *Fgr*GalOx (Table 1). Despite the obvious disruption of the hydrophobic wall (Fig. S27-E), *Fox*GalOxB possesses predominant GalOx activity, albeit with a low turnover rate. Although this modeled complex precludes definitive analysis in the absence of site-directed mutagenesis and kinetic analysis of variants, it is notable that the low turnover rate observed for *Fox*GalOxB is matched by a low K_M value. The same hydrogen bonds between galactose, arginine, and tryptophan indicated in other enzymes are maintained in *Fox*GalOxB, consistent with this observation (Table S11).

In addition to the obvious residues lining the active site pocket, W290 in *Fgr*GalOx is a second shell amino acid which strongly affects catalysis in AA5_2 CROs. *Fgr*GalOx W290 stacks with the tyrosine-cysteine crosslinked radical cofactor that is central to the mechanism of CROs, and potentially makes a hydrogen bond to the ring oxygen of galactose (Fig. 4). Mutagenesis of W290 significantly diminishes catalytic efficiency [73]. The homologs *Cgr*AAO and *Cgr*AlcOx possess, respectively, a tyrosine and a phenylalanine at this position, and site-directed mutagenesis of either to tryptophan modulates the relative activities toward carbohydrates versus other primary alcohols [37, 39]. On the other hand, the recently characterized *Fgr*AAO and *Fox*AAO both possess a tryptophan at the same position, but yet have much higher catalytic efficiencies on aryl alcohols than galactose [40]. As such, the presence of this tryptophan as a galactose specificity determinant is somewhat ambiguous. However, we note that three general alcohol oxidases (*Por*AlcOx, *Cgl*AlcOx, and *Asy*AlcOx) and the two raffinose oxidases (*Uma*RafOx, *Phu*RafOx), all of which showed low or no activity on galactose (< 3 μmol min^{-1} mg^{-1}) do not carry a tryptophan at this position. *Por*AlcOx, *Cgl*AlcOx, and *Asy*AlcOx all have a phenylalanine at this position, while the raffinose oxidases have a tyrosine (Table 1). Other enzymes in our study capable of galactose oxidation all have retained this tryptophan residue, like the archetypal *Fgr*GalOx. In this context, it is notable that a CRO from *Streptomyces lividans* is poorly active on galactose, yet contains a corresponding secondary shell tryptophan whose presence is critical to the formation of the cysteine-tyrosine crosslink [93, 94]. In this enzyme, the indole ring of the tryptophan is oriented differently compared to *Fgr*GalOx, which may affect specificity through electronic effects and/or altered hydrogen bonding with the substrate [93, 94].

The last amino acid that warrants comment is C383, which lies at the back of the active site pocket but does not directly interact with galactose in *Fgr*GalOx. This residue has been shown previously to affect *Fgr*GalOx catalytic efficiency on galactose [71], as its replacement with a serine increased the activity of the resulting mutant while an asparagine substitution decreased the activity tenfold [40, 71]. X-ray crystallography demonstrated that the C383S mutant of *Fgr*GalOx participates in a H-bonded water network, stabilizing the backbone nitrogen between residues Tyr495 and His496 and possibly increasing its activity [74]. In our study, *Afl*AlcOx, *Pru*AA5_2A (*Pru*AlcOx), and *Pfe*GalOx have some of the highest catalytic efficiencies from all enzymes produced and they all natively have this C383S substitution (Table 1). Furthermore, *Mre*GalOx has the same active site structure as *Exe*GalOx but displays a tenfold decreased catalytic efficiency on galactose (Table 2). Contrary to *Exe*GalOx, *Mre*GalOx has an asparagine instead of a cysteine at the position corresponding to C383 in *Fgr*GalOx which, due to a bulkier side chain, could disrupt the hydrogen bonding network, thereby lowering the activity of the enzyme.

Although the contributions of individual active-site amino acids to the specificity of AA5_2 CROs is not completely

unambiguous, we can nonetheless discern some general trends based on kinetic observations for the complete set of enzymes characterized to date (based on *Fgr*GalOx residue numbering): the presence of R330 is crucial for low K_M values on galactose and galactosides, while its replacement generally favors non-carbohydrate oxidation. The neighboring amino acid, Y329, is not a key determinant of galactose oxidase binding/activity and a variety of amino acid residues are found at this position in CROs (Fig. S1-F). In contrast, F194 is important for efficient turnover rates toward galactose and although this amino acid is mostly conserved among AA5_2 sequences (Fig. S1-D), a majority of other sequences, regardless of carbohydrate or non-carbohydrate activity, contain an aromatic residue at this position likely to maintain the hydrophobic wall with F464. Lastly, the presence of W290 allows for prominent galactose oxidase activity but does not absolutely dictate enzyme specificity, possibly because spatial orientation of the indole ring in the secondary shell may be an addition contributor to substrate specificity [93, 94], which cannot be assessed on the basis of sequence alone.

Conclusion

A growing body of functional information on AA5_2 members, including the detailed biochemical characterization of twelve fungal orthologs in the present study, continues to reveal a surprisingly broad catalytic diversity within this family of CROs. In this context, we note that automated genome annotations often label AA5_2 members as "galactose oxidases" based on sequence similarity to the archetype *Fgr*GalOx, which misrepresents the wider potential of these enzymes. Thus, such annotations should be viewed with caution, and we would generally advocate that these proteins should be more conservatively annotated as "copper radical oxidases" [34] until specificity can be reasonably established. We also note that the true physiological substrates of these enzymes are generally unknown, so specificities determined in vitro—including those here—may only be indicative. Nonetheless, it is revealing that AA5_2 comprises apparent galactose oxidases, raffinose oxidases, broad-spectrum alkyl- and aryl-alcohol oxidases, and non-carbohydrate alcohol oxidases of potential use in the specific biocatalytic transformation of both carbohydrate and non-carbohydrate substrates, including bioproducts, such as HMF and glycerol.

The replacement of chemical oxidants with redox enzymes is a topic of considerable contemporary interest, for which the palette of CROs constitutes an alternative to cofactor-dependent oxidases [60]. For example, *Cgl*AlcOx has the highest catalytic efficiency on HMF currently reported, compared to *Cgr*AAO [39] and *Fgr*AAO [40], the bacterial HMF oxidase (a GMC superfamily oxidoreductase) [95], and some glyoxal oxidases from AA5_1 (Table S12) [87, 96, 97]. On the other hand, *Afl*AlcOx may find use in multiple biocatalytic processes because it has high activity on both carbohydrate and non-carbohydrate substrates. The optimal choice of enzyme for a specific biocatalytic application will of course be substrate dependent, for which the current palette of AA5_2 CROs serves as an immediate resource and a starting point for future enzyme engineering efforts.

Materials and Methods

Chemicals and enzymes

Ultrapure water was used for the preparation of all buffers and stock solutions unless stated otherwise. Catalase from bovine liver (2000–5000 units per mg protein, Sigma) and horseradish peroxidase (Rz > 3, 300 units per mg, Bio Basic Canada Inc.), obtained as lyophilized powders, were used as received. Other substrates and reagents were purchased from commercial sources (Sigma-Aldrich, VWR or Fisher) and used without further purification.

Sequence analysis and bioinformatics

A total of 247 bacterial and 103 fungal AA5_2 sequences were collected from the CAZy database in January 2019 [17]. Sequences of characterized AA5_1 members were also retrieved from the CAZy database. In addition, full-length sequences of *Fgr*GalOx (Uniprot P0CS93), *Cgr*AlcOx (GenBank EFQ30446), and *Cgr*AAO (GenBank EFQ27661), as well as their corresponding catalytic domains, were used as templates for BLAST analysis against all Fungi in the Joint Genome Institute MycoCosm portal (https://genome.jgi.doe.gov/programs/fungi/index.jsf) [98, 99]. Where present, signal peptides and additional modules, such as carbohydrate-binding modules, were removed to isolate the catalytic modules for subsequent analysis. Catalytic modules sharing 100% identity were down-sampled to one sequence to eliminate redundancy. A multiple sequence alignment was created with MAFFT v.7.402 using the L-INS-I algorithm [100], on the CIPRES Science Gateway (www.phylo.org) [101]. Using this alignment, catalytic modules having deletions/substitutions at key active-site residues, namely, Cys272 and Tyr316 (which form the crosslinked thioether-tyrosyl cofactor) and other copper coordinating residues of *Fgr*GalOx [36] were removed. Moreover, obviously erroneous sequences generated by incorrect splicing predictions were removed through identification of unusually long deletions/insertions.

With this curated multiple sequence alignment, comprising 623 AA5_2 catalytic modules, a maximum likelihood phylogenetic tree was produced using RAxML v.8, with

100 bootstrap replications [102], on the CIPRES Science Gateway portal. The resulting tree was visualized using FigTree and monophyletic groups were supported by bootstrap values > 60 and tree topology. SSNs were generated by computing BLASTP [103] all-versus-all local alignments of the curated 623 AA5_2 catalytic domains using SSNpipe (https://github.com/ahvdk/SSNpipe), which generated the *E*-value, bit score, alignment length, sequence identity, and sequence similarity for all sequence pairs. The data were filtered using a bit score threshold between 500 and 600, with increments of 25, to generate the final SSNs. A bit score threshold of 550, clustering the sequences into groups, which resolves the same monophyletic groups as those observed in the phylogenetic tree, was retained. The SSNs were visualized with Cytoscape using yFiles Organic Layout [104], and coloring of each node was based on monophyletic groups inferred from the phylogenetic tree.

In addition, Phyre2 [105] was used to make three-dimensional homology models for *Afl*AlcOx, *Pru*AA5_2A (*Pru*-AlcOx), *Pfe*GalOx, *Exe*GalOx, *Fox*GalOxB, *Fox*AlcOx, and *Mre*GalOx. The structural models were aligned to the crystal structures of *Fgr*GalOx (PDB ID 1GOF) [92] and *Cgr*AlcOx (PDB ID 5C86) [37] for spatial amino acid comparison to give further support to the alignment.

DNA cloning

cDNA encoding genes of interest without the predicted native signal peptide, and including a C-terminal His6 tag-encoding sequence, were commercially synthesized in a codon-optimized form (BioBasic, Markham, Canada) and cloned directly into pPICZα-A or pPICZα-C using the EcoRI, SfiI, ClaI, XbaI, and NotI restriction sites flush with the sequence encoding the *S. cerevisiae* α-factor signal peptide. The resultant constructs were transformed into chemically competent *E. coli* DH5α by heat shock.

Recombinant strain production

All recombinant proteins were produced using the in-house 3PE Platform (*Pichia Pastoris* Protein Express www.platform3pe.com) as described in Haon et al., [106]. The transformations of competent *P. pastoris* X33 cells with 5 µg of PmeI-linearized pPICZα-A plasmids (Invitrogen, Cergy-Pontoise, France) containing the targeted sequences were done by electroporation. Each construction was spread on plates containing either 100 or 500 µg mL^{-1} of Zeocin, and three *P. pastoris* transformants were isolated from each plate. Zeocin-resistant *P. pastoris* transformants were then screened for protein expression in 24-deepwell plates with the following conditions: induction of expression was done for 3 d at 25 °C in BMMY supplemented with $CuSO_4$ (500 µM) and methanol (3%, v/v), with daily addition of 1% (v/v) methanol. The recombinant proteins were then purified from supernatant by affinity chromatography on Ni–NTA resin using automated procedure as described previously [106]. Finally, the analysis of purified recombinant protein expression by SDS-PAGE (8% polyacrylamide pre-cast E-PAGE gels, Invitrogen) using Coomassie blue staining was used to select the best-producing transformants.

Small-scale protein production and purification

The best-producing transformants were streaked on yeast extract peptone dextrose (YPD) agar plates containing Zeocin (100 µg mL^{-1}) and allowed to grow 3 d (30 °C). One colony of the selected transformants served to inoculate 5 mL of YPD broth in 50 mL sterile conical tubes and were incubated for 5 h at 30 °C and 160 rpm in an orbital shaker. The preculture was used to inoculate (0.2%, v/v) 500 mL of BMGY, before incubation for 16 h (30 °C) until the OD600 nm reached 4–6. Then, the biomass was harvested by centrifugation (10 min, 16 °C, 5000*g*) and resuspended in 100 mL of BMMY medium supplemented with 500 µM of $CuSO_4$ and 3% methanol (v/v) and incubated for 3 d in an orbital shaker (200 rpm, 25 °C), with daily feeding of 1% methanol (v/v). For *Por*AlcOx, *Sto*AA5, and *Cca*AA5 clones, proteins expression was further improved by lowering induction temperature to 20 °C and increasing daily methanol feed to 3% (v/v). The cells were then harvested by centrifugation (10 min, 4 °C, 5000*g*); the supernatants were filtered on 0.45 µm membrane (Millipore, Burlington, Massachusetts, USA) and stored at 4 °C prior to purification.

The filtered supernatants were adjusted to pH 7.8 just before purification, filtered on 0.22 µm filters (Millipore, Molsheim, France), and loaded onto a His*Trap* HP-5 mL column (GE Healthcare, USA), equilibrated with buffer A (Tris–HCl 50 mM, pH 7.8, NaCl 150 mM, imidazole 10 mM) and connected to an Äkta Xpress system (GE Healthcare). (His)6-tagged recombinant proteins were eluted with 50% buffer B (Tris–HCl 50 mM pH 7.8, NaCl 150 mM, imidazole 500 mM). After SDS-PAGE (10% polyacrylamide pre-cast gel, Bio-Rad) analysis, fractions containing the recombinant enzymes were pooled, concentrated, and exchanged to 50 mM Tris–HCl pH 7.0. The concentrated proteins were incubated overnight at 4 °C with 1 mM $CuSO_4$ to ensure full copper loading and then buffer exchanged in 50 mM Tris–HCl buffer pH 7.0 to remove $CuSO_4$ excess. The protein concentration was determined by UV absorption at 280 nm using a Nanodrop ND-200 spectrophotometer (Thermo Fisher Scientific, USA) and calculated using theoretical molecular weight and molar extinction coefficients determined with ProtParam web tool (https://web.expasy.org/protparam/) (*Exe*GalOx $\varepsilon = 142{,}522$ M^{-1} cm^{-1}; *Mre*GalOx $\varepsilon = 153{,}842$ M^{-1} cm^{-1}; *Fox*GalOxB $\varepsilon = 140{,}907$ M^{-1} cm^{-1}; *Pfe*GalOx $\varepsilon = 131{,}967$ M^{-1} cm^{-1};

*Uma*RafOx $\varepsilon = 109{,}062\ M^{-1}\ cm^{-1}$; *Phu*RafOx $\varepsilon = 105{,}052\ M^{-1}\ cm^{-1}$; *Afl*AlcOx $\varepsilon = 134{,}885\ M^{-1}\ cm^{-1}$; *Pru*AA5_2A (*Pru*AlcOx) $\varepsilon = 126{,}802\ M^{-1}\ cm^{-1}$; *Fox*AlcOx $\varepsilon = 131{,}967\ M^{-1}\ cm^{-1}$; *Por*AlcOx $\varepsilon = 89{,}645\ M^{-1}\ cm^{-1}$; *Cgl*AlcOx $\varepsilon = 95{,}527\ M^{-1}\ cm^{-1}$; *Asy*AlcOx $\varepsilon = 123{,}947\ M^{-1}\ cm^{-1}$; *Cca*AA5 $\varepsilon = 77{,}475\ M^{-1}\ cm^{-1}$; *Sto*AA5 $\varepsilon = 69{,}455\ M^{-1}\ cm^{-1}$).

Large-scale protein production and purification

The large-scale protein production and purification were performed as previously published [40]. Briefly, single colonies of *P. pastoris* X33 expressing clones were streaked onto agar plates containing Zeocin and grown for 2 d in the dark in a 30 °C incubator. Precultures with 5 mL of YPD and 0.4 mg mL^{-1} Zeocin were inoculated using a single colony and shaken at 30 °C at 250 rpm for 9 h. Biomass production was initiated by the addition of the preculture into 1 L of BMGY media and shaken in 4 L flasks at 250 rpm overnight at 30 °C. Once the BMGY cultures reached an OD_{600} of 6–12, the cells were harvested by centrifugation at 3000*g* for 15 min at room temperature. Subsequently, the cells were resuspended using 400 mL of BMMY media, supplemented with 0.5 mM copper sulfate, containing 3% methanol and transferred to 1 L flasks. The flasks were shaken at 250 rpm at 16 °C for 3 d. The cultures were fed 1% (v/v) methanol every 24 h and on day three, the secreted proteins were separated from the cells by centrifugation at 8000*g* for 15 min at 4 °C. The supernatant was decanted, filtered through 0.45 µm membrane and the pH of the liquid medium was raised to 7.5–8.0 by dropwise addition of 1 M NaOH to the stirred solution. Subsequently, the liquid media which contained the proteins of interest were filtered again through a 0.45 µm membrane and allowed to equilibrate for at least 12 h at 4 °C.

The supernatant was loaded into a 5 mL pre-packed Ni–NTA column, pre-equilibrated with 50 mM sodium phosphate buffer at pH 7.5, containing 300 mM NaCl and 10 mM imidazole, at 5 mL min^{-1}. The column was washed with 10 column volumes of equilibration buffer (50 mM sodium phosphate, 300 mM NaCl, 10 mM imidazole at pH 7.5) at 5 mL min^{-1}. Proteins were eluted with a linear gradient from 2 to 100% of 500 mM imidazole in 50 mM sodium phosphate buffer, 300 mM NaCl, and pH 7.5 at 5 mL min^{-1}. The total elution volume was 125 mL collected in 1 mL fractions. The fractions of interest were pooled and further desalted using a Sephadex G-25 column pre-equilibrated with 50 mM sodium phosphate buffer at pH 7.5 at 5 mL min^{-1}. A total volume of 200 mL of equilibration buffer was passed through the column at 5 mL min^{-1}. The fractions of interest were pooled and concentrated using a 30,000 MWCO Vivaspin centrifugal concentrator. The proteins were aliquoted, flash frozen in liquid nitrogen, and stored at −70 °C. SDS-PAGE was performed using pre-cast 4–20% (w/v) polyacrylamide gel in the presence of 2% (w/v) SDS under reducing conditions. Proteins were visualized using Coomassie blue R-250 and molecular weights were estimated using a standard curve of the log (MW) versus Rf of the protein ladder (BLUelf). Protein concentrations were determined by measuring A_{280}. The extinction coefficients were calculated using the ProtParam tool on the ExPASy server.

Analytical protein deglycosylation

The presence of protein glycosylation on *Uma*RafOx, *Phu*RafOx, *Afl*AlcOx, *Pru*AA5_2A (*Pru*AlcOx), *Exe*GalOx, *Mre*GalOx, *Pfe*GalOx, *Fox*GalOxB, *Fox*AlcOx, *Cgl*AlcOx, *Asy*AlcOx, *Por*AlcOx, *Sto*AA5, and *Cca*AA5 was assessed by treatment with N-glycosidase F from *Flavobacterium meningosepticum* (PNGaseF, New England Biolabs) according to the manufacturer's protocol. Briefly, deglycosylation experiments were performed under denaturing condition by adding 5 µg of protein to 10X Glycoprotein Denaturing Buffer and heated for 10 min at 100 °C. The samples were subsequently diluted to 20 µL with GlycoBuffer 2 and tertigol-type NP-400 detergent. Finally, 1 µL of PNGaseF was added to the sample and incubated for 1 h at 37 °C. Changes in protein mobility were assessed by SDS-PAGE stained with Coomassie blue R-250. Molecular weights of proteins were estimated using a standard curve of the log (MW) versus Rf of the protein ladder (BLUelf).

Initial activity test

The colorimetric HRP–2,2'-azinobis(3-ethylbenzthiazoline-6-sulfonic acid (ABTS)-coupled assay was used to determine the kinetics of the enzymatic oxidation of substrate. The oxidation of the alcohol group on the substrates by AA5 enzymes consumes 1 equivalent of O_2 and produces 1 equivalent of H_2O_2. The oxidation of ABTS ($\lambda_{max} = 514$ nm, ε—36,000 $M^{-1}\ cm^{-1}$) [107] is catalyzed by the enzyme HRP using 2 equivalents of H_2O_2. This is a standard assay used to monitor initial rate kinetics for AA5 enzymes [79]. This assay was optimized for sensitivity and linearity. The enzymes that expressed well from the production screen were tested for activity on 300 mM galactose, 300 mM raffinose, and 30 mM benzyl alcohol. Enzyme activity was measured using the HRP-ABTS-coupled assay in 100 mM sodium phosphate buffer at pH 8.0, 0.46 mM ABTS, and 21 U mL^{-1} of HRP at 30 °C using a Cary 60 UV–Vis spectrometer.

Plate assays—proof of concept

The enzyme *Afl*AlcOx was used for the proof-of-concept experiments for the development of a medium throughput

plate-based HRP-ABTS-coupled assay. The pH profile, temperature stability profile, and partial substrate screen for *Afl*AlcOx were performed initially using the standard HRP-ABTS-coupled assay using a Cary 60 UV–Vis spectrometer with plastic 1 mL cuvettes (Fig. S4). The same experiments using the same conditions were subsequently performed using a 96-well plate assay with BioTek Epoch microplate spectrophotometer. All experiments with *Afl*AlcOx performed on the Cary 60 UV–Vis spectrometer were equivalent to experiments performed using the BioTek Epoch microplate spectrophotometer (Fig. S4), validating the plate assay. This assay was optimized for sensitivity and linearity. A standard curve for the production of ABTS radical was performed by incubating 7 mM ABTS with 12.25–22.05 nmol potassium persulfate for 16 h in the dark to correctly assess the pathlength of the 96-well plate [107] (Fig. S3).

pH-activity profile

Enzyme activity across a wide range of pH values was determined using phosphate-citrate (pH 4.0–7.0), sodium phosphate (pH 5.5–8.5), glycine–NaOH (pH 8.5–11.0), and CHES (pH 8.5–10.50) buffers. Enzyme activity was measured using the HRP-ABTS-coupled assay in a 96-well plate assay at RT in 100 mM buffer with either 300 mM of galactose, 30 mM benzyl alcohol, or 300 mM of glycerol depending on the initial activity screen test.

Temperature stability

Temperature stability of candidate enzymes was determined by first diluting the stock protein in 50 mM sodium phosphate buffer at the previously optimum pH determined for each enzyme in the presence of 0.1 mg ml^{-1} of bovine serum albumin (BSA). The diluted protein was then pre-incubated in a thermocycler at 30 °C, 39 °C, 49 °C, 60 °C, 69 °C, and 79 °C. Samples were taken out at different time intervals and the activity of the proteins was measured using the HRP-ABTS-coupled assay in a 96-well plate assay at RT with 300 mM galactose, 30 mM benzyl alcohol, or 300 mM glycerol as the substrate based on previous experiments.

Substrate screen

The activity of candidate enzymes was surveyed on a variety of substrates using the HRP-ABTS-coupled assay in 100 mM sodium phosphate buffer at pH value determined by the pH profile, 0.46 mM ABTS, and 21 U mL^{-1} of HRP at RT with the 96-well plate assay method. The initial substrate screen included carbohydrates, polyols, diols, and primary alcohol substrates at 300 mM, benzyl alcohol and galactitol at 30 mM, methyl glyoxal and glycolaldehyde dimer at 5 mM, and aryl alcohols and furans at 2.5 mM. One unit of AA5 enzyme activity was defined as the amount of enzyme required to oxidize 2 µmol of ABTS per minute, which is equivalent to the consumption of 1 µmol of oxygen per minute.

Michaelis–Menten Kinetics

To determine Michaelis–Menten parameters of candidate enzymes, different concentrations of substrate solutions were used over the range of 0.1–1,500 mM for galactose, 0.5–750 mM for melibiose, 0.1–285 mM for benzyl alcohol, 0.5–200 mM for butanol, 5–6000 mM glycerol, 0.1–200 mM 1,4-butanediol, and 0.01–25 mM HMF. The reactions were performed using the HRP-ABTS-coupled assay with 0.46 mM ABTS, 21 U mL^{-1} of HRP at different temperatures in 100 mM buffer at different pH informed by the temperature stability assays and pH profile experiments using the Cary 60 UV–VIS spectrometer with plastic 1 mL cuvettes. More detailed information for the experimental conditions of each Michaelis–Menten experiment is given in Table 4. Data were fit with the Michaelis – Menten equation using OriginPro software (OriginLab 9.55).

Computational docking studies

Molecular docking simulations were performed using the CHIMERA software from UCSF Resource for Biocomputing, Visualization, and Informatics [108]. The *Fgr*GalOx crystal structure (PDB ID 1GOF) and a Phyre model of *Afl*AlcOx, *Pru*AA5_2A (*Pru*AlcOx), *Pfe*GalOx, *Exe*GalOx, *Fox*GalOxB, and *Fox*AlcOx were used to generate the receptors for simulations. Galactose was extracted from a different PDB file (PDB ID 1SO0). Ligands and receptors were first prepared for docking in chimera by adding hydrogens and assigning proper protonation states. The docking simulation itself was performed using Autodock VINA, run within CHIMERA, with the AMBER03 force field [109]. Appropriate simulation cells were defined for the respective docking simulations. For docking of galactose, a 7 Å, 6 × 6 × 7 Å, or a 6 Å cell with the copper atom bordering the z-coordinate edge was chosen. Galactose gave reasonable binding poses with all enzymes used. The modelled receptor–ligand complex structures were analyzed using the PyMOL software (Schrodinger LLC) to determine ligand–receptor interactions, including bond distances.

Enzyme product analysis

Oxidation of HMF, DFF, HMFCA, and FDCA

Oxidation of furan-containing compounds with AA5_2 enzymes was performed as previously published [40]. Ten mM of substrate (HMF, DFF, HMFCA, and FDCA) and 1 mg mL^{-1} of both catalase and HRP were combined and the reaction was initiated by adding 60 µg of purified AA5_2 enzyme to a vial with 50 mM buffer in a final volume of 1 mL. Reactions were stirred at 400 rpm at room temperature for 17 h followed by enzyme removal through ultrafiltration (5 kDa cut-off Vivaspin Sartorius, Stonehouse, UK). D_2O was added to the filtrate to a final composition of 10% (v/v). NMR experiments were performed on a Bruker AVANCE 600 MHz spectrometer. ^1H NMR spectra were collected with water suppression (4.7 ppm) using a standard pre-saturation pulse sequence. Chemical shifts were calibrated to the internal HOD peak (4.7 ppm). Standards of all substrates were used to identify distinct chemical shifts for each molecule. Integration values of relevant peak areas were used to determine conversion percentages.

Oxidation of glycerol

Oxidation of glycerol and subsequent product analysis was performed as previously published [40]. 0.54 M glycerol and 1 mg mL^{-1} of both catalase and HRP were combined and 700 µg of purified AA5_2 enzyme in a final volume of 1 mL (50 mM buffer) was added to start the reaction. Reactions were stirred at 400 rpm at room temperature for 24 h, and subsequently, the enzymes were removed by ultrafiltration (5 kDa cut-off Vivaspin Sartorius, Stonehouse, UK). 20 mg of 2,4-dinitrophenyl hydrazine was added to the reaction mixtures, which were incubated in a heat block at 50 ℃ for 6 h with intermittent shaking. A TLC plate was used to check formation of desired product (Rf = 0.46, 100% EtOAc). The solution was purified via preparatory TLC and the desired hydrazone was mechanically isolated and dissolved in MeOH. Subsequently, the solution was filtered and concentrated and the composition of the purified glyceraldehyde-hydrazones was analyzed by HPLC (3 µL injection, Chiracel® IA-3). Eluents used for HPLC methods, i.e. water with 0.1% formic acid (A) and methanol (B), were LC–MS grade (Optima, Fisher). For separation between L-and D-glyceraldehyde-hydrazones an isocratic method using 60% A, 40% B with a flow rate of 0.65 mL min^{-1} was used with a 12 min stop time with UV detection at 360 nm. L-glyceraldehyde-hydrazone eluted at 2.30 min and D-glyceraldehyde-hydrazone eluted at 2.76 min. ESI mass spectra were also collected in positive mode scan for *m/Z* 95–500 running at 0.8 s/cycle, drying gas = 5.0 L min^{-1}, nebulizer pressure = 50 psi, gas temperature = 300 °C, and capillary voltage = 4000 V.

Supplementary Information The online version contains supplementary material available at https://doi.org/10.1007/s00018-021-03981-w.

Acknowledgements The authors thank Dr. Maria Ezhova and Dr. Zhicheng (Paul) Xia (UBC Department of Chemistry) for support with NMR data acquisition.

Author contributions MC performed enzyme cloning, biochemistry, enzyme kinetic and product analysis, all corresponding data analysis, and drafted the manuscript; YM performed sequence analysis, bioinformatics, and enzyme cloning, wrote portions of manuscript, and revised the manuscript; DR and MH performed recombinant protein production and initial kinetic measurements; PM and JH assisted with the glycerol oxidation experiments; ML and JGB assisted with data analysis; and HB coordinated research, analyzed data, and revised the manuscript with input from all the authors.

Funding Funding is gratefully acknowledged from: The Natural Sciences and Engineering Research Council of Canada (NSERC) Discovery Grants RGPIN 435223-13 and RGPIN-2018–03892; NSERC Strategic Partnership Grant NETGP 451431-13 for the "NSERC Industrial Biocatalysis Network"; NSERC Strategic Partnership Grant (STPGP 493781–16) and joint Agence Nationale de la Recherche grant (ANR-17-CE07-0047), "FUNTASTIC—Fungal copper radical oxidases as new biocatalysts for the valorization of biomass carbohydrates and alcohols"; and Genome Canada/Genome BC/Ontario Genomics/Genome Quebec for the Large-Scale Applied Research Project (LSARP, project #10405), "SYNBIOMICS—Functional genomics and techno-economic models for advanced biopolymer synthesis").

Data availability All data generated or analyzed during this study are included in this published article and its supplementary information files. All nucleotide sequence, protein sequence, and protein structural information used in this work were extracted from existing accessions in public databases, i.e., GenBank, Joint Genome Institute MycoCosm portal, and the Protein Data Bank.

Declarations

Conflict of interests The authors declare that they have no competing interests.

Ethics approval and consent to participate Not applicable.

Consent for publication Not applicable.

References

1. Cook J, Oreskes N, Doran P, Anderegg W, Verheggen B, Maibach E, Carlton J, Lewandowsky S, Skuce A, Green S, Nuccitelli D, Jacobs P, Richardson M, Winkler B, Painting R, Rice K (2016) Consensus on consensus: a synthesis of consensus estimates on human-caused global warming. Environ Res Lett 11:048002. https://doi.org/10.1088/1748-9326/11/4/048002
2. Tollefson J (2018) Can the world kick its fossil-fuel addiction fast enough? Nature 7702:422–425. https://doi.org/10.1038/d41586-018-04931-6

3. Fabian N (2015) Economics: Support low-carbon investment. Nature 519:27–29. https://doi.org/10.1038/519027a
4. Zhang YHP (2011) What is vital (and not vital) to advance economically-competitive biofuels production. Process Biochem 46(11):2091–2110. https://doi.org/10.1016/j.procbio.2011.08.005
5. Naik SN, Goud VV, Rout PK, Dalai AK (2010) Production of first and second generation biofuels: a comprehensive review. Renewable Sustainable Energy Rev 14(2):578–597. https://doi.org/10.1016/j.rser.2009.10.003
6. Hayes DJM (2013) Second-generation biofuels: Why they are taking so long. WIREs Energy Environ 2(3):304–334. https://doi.org/10.1002/wene.59
7. Bender TA, Dabrowski JA, Gagné MR (2018) Homogeneous catalysis for the production of low-volume, high-value chemicals from biomass. Nat Rev Chem 2(5):35–46. https://doi.org/10.1038/s41570-018-0005-y
8. Fatih DM (2009) Biorefineries for biofuel upgrading: a critical review. Appl Energy 86(Supplement 1):S151–S161. https://doi.org/10.1016/j.apenergy.2009.04.043
9. Ragauskas AJ, Williams CK, Davison BH, Britovsek G, Cairney J, Eckert CA, Frederick WJ, Hallett JP, Leak DJ, Liotta CL, Mielenz JR, Murphy R, Templer R, Tschaplinski T (2006) The path forward for biofuels and biomaterials. Science 311(5760):484–489. https://doi.org/10.1126/science.1114736
10. Dessbesell L, Xu C, Pulkki R, Leitch M, Mahmood N (2017) Forest biomass supply chain optimization for a biorefinery aiming to produce high-value bio-based materials and chemicals from lignin and forestry residues: a review of literature. Can J For Res 47(3):277–288. https://doi.org/10.1139/cjfr-2016-0336
11. Allais F, Coqueret X, Farmer T, Raverty W, Rémond C, Paës G (2020) Editorial: From biomass to advanced bio-based chemicals & materials: a multidisciplinary perspective. Front Chem 8(131). https://doi.org/10.3389/fchem.2020.00131
12. Goswami P, Chinnadayyala SSR, Chakraborty M, Kumar AK, Kakoti A (2013) An overview on alcohol oxidases and their potential applications. Appl Microbiol Biotechnol 97(10):4259–4275. https://doi.org/10.1007/s00253-013-4842-9
13. Hernández-Ortega A, Ferreira P, Martínez AT (2012) Fungal aryl-alcohol oxidase: a peroxide-producing flavoenzyme involved in lignin degradation. Appl Microbiol Biotechnol 93(4):1395–1410. https://doi.org/10.1007/s00253-011-3836-8
14. Hollmann F, Arends IWCE, Buehler K, Schallmey A, Bühler B (2011) Enzyme-mediated oxidations for the chemist. Green Chem 13(2):226–265. https://doi.org/10.1039/C0GC00595A
15. Horn SJ, Vaaje-Kolstad G, Westereng B, Eijsink VG (2012) Novel enzymes for the degradation of cellulose. Biotechnol Biofuels 5(1):45. https://doi.org/10.1186/1754-6834-5-45
16. Johansen KS (2016) Discovery and industrial applications of lytic polysaccharide mono-oxygenases. Biochem Soc Trans 44(1):143–149. https://doi.org/10.1042/BST20150204
17. Levasseur A, Drula E, Lombard V, Coutinho PM, Henrissat B (2013) Expansion of the enzymatic repertoire of the CAZy database to integrate auxiliary redox enzymes. Biotechnol Biofuels 6(1):41. https://doi.org/10.1186/1754-6834-6-41
18. Lombard V, Golaconda Ramulu H, Drula E, Coutinho PM, Henrissat B (2013) The carbohydrate-active enzymes database (CAZy) in 2013. Nucleic Acids Res 42(D1):D490–D495. https://doi.org/10.1093/nar/gkt1178
19. Artzi L, Bayer EA, Moraïs S (2017) Cellulosomes: bacterial nanomachines for dismantling plant polysaccharides. Nat Rev Microbiol 15(2):83–95. https://doi.org/10.1038/nrmicro.2016.164
20. Payne CM, Knott BC, Mayes HB, Hansson H, Himmel ME, Sandgren M, Ståhlberg J, Beckham GT (2015) Fungal cellulases. Chem Rev 115(3):1308–1448. https://doi.org/10.1021/cr500351c
21. Murphy C, Powlowski J, Wu M, Butler G, Tsang A (2011) Curation of characterized glycoside hydrolases of fungal origin. Database 2011:bar020. https://doi.org/10.1093/database/bar020
22. Basit A, Liu J, Rahim K, Jiang W, Lou H (2018) Thermophilic xylanases: from bench to bottle. Crit Rev Biotechnol 38(7):989–1002. https://doi.org/10.1080/07388551.2018.1425662
23. Ryu DDY, Mandels M (1980) Cellulases: biosynthesis and applications. Enzyme Microb Technol 2(2):91–102. https://doi.org/10.1016/0141-0229(80)90063-0
24. Tomme P, Warren RAJ, Gilkes NR (1995) Cellulose Hydrolysis by Bacteria and Fungi. In: Poole RK (eds) Advances in microbial physiology. Academic Press, pp 1–81. https://doi.org/10.1016/S0065-2911(08)60143-5
25. Davies G, Henrissat B (1995) Structures and mechanisms of glycosyl hydrolases. Structure 3(9):853–859. https://doi.org/10.1016/S0969-2126(01)00220-9
26. Møller MS, Svensson B (2016) Structural biology of starch-degrading enzymes and their regulation. Curr Opin Struct Biol 40:33–42. https://doi.org/10.1016/j.sbi.2016.07.006
27. Knob A, Terrasan CRF, Carmona EC (2010) β-Xylosidases from filamentous fungi: an overview. World J Microbiol Biotechnol 26(3):389–407. https://doi.org/10.1007/s11274-009-0190-4
28. Juturu V, Wu JC (2012) Microbial xylanases: engineering, production and industrial applications. Biotechnol Adv 30(6):1219–1227. https://doi.org/10.1016/j.biotechadv.2011.11.006
29. Friedl A (2012) Bioethanol from starch. In: Meyers RA (ed) Encyclopedia of sustainability science and technology. Springer, New York, NY, pp 987–1001. https://doi.org/10.1007/978-1-4419-0851-3_432
30. Schoemaker HE, Mink D, Wubbolts MG (2003) Dispelling the myths–biocatalysis in industrial synthesis. Science 299(5613):1694–1697. https://doi.org/10.1126/science.1079237
31. Bornscheuer UT, Huisman GW, Kazlauskas RJ, Lutz S, Moore JC, Robins K (2012) Engineering the third wave of biocatalysis. Nature 485(7397):185–194. https://doi.org/10.1038/nature11117
32. Wu S, Snajdrova R, Moore JC, Baldenius K, Bornscheuer UT (2021) Biocatalysis: enzymatic synthesis for industrial applications. Angew Chem Int Ed 60(1):88–119. https://doi.org/10.1002/anie.202006648
33. Whittaker JW (2003) Free radical catalysis by galactose oxidase. Chem Rev 103(6):2347–2364. https://doi.org/10.1021/cr020425z
34. Kersten P, Cullen D (2014) Copper radical oxidases and related extracellular oxidoreductases of wood-decay Agaricomycetes. Fungal Genet Biol 72:124–130. https://doi.org/10.1016/j.fgb.2014.05.011
35. Whittaker MM, Kersten PJ, Nakamura N, Sanders-Loehr J, Schweizer ES, Whittaker JW (1996) Glyoxal oxidase from *Phanerochaete chrysosporium* is a new radical-copper oxidase. J Biol Chem 271(2):681–687. https://doi.org/10.1074/jbc.271.2.681
36. Ito N, Phillips SEV, Stevens C, Ogel ZB, McPherson MJ, Keen JN, Yadav KDS, Knowles PF (1991) Novel thioether bond revealed by a 1.7 Å crystal structure of galactose oxidase. Nature 350(6313):87–90. https://doi.org/10.1038/350087a0
37. Yin D, Urresti S, Lafond M, Johnston EM, Derikvand F, Ciano L, Berrin J-G, Henrissat B, Walton PH, Davies GJ, Brumer H (2015) Structure–function characterization reveals new catalytic diversity in the galactose oxidase and glyoxal oxidase family. Nat Commun 6(1):10197. https://doi.org/10.1038/ncomms10197
38. Oide S, Tanaka Y, Watanabe A, Inui M (2019) Carbohydrate-binding property of a cell wall integrity and stress response component (WSC) domain of an alcohol oxidase from the rice blast pathogen *Pyricularia oryzae*. Enzyme Microb Technol 125:13–20. https://doi.org/10.1016/j.enzmictec.2019.02.009
39. Mathieu Y, Offen WA, Forget SM, Ciano L, Viborg AH, Blagova E, Henrissat B, Walton PH, Davies GJ, Brumer H (2020) Discovery of a fungal copper radical oxidase with high catalytic

efficiency toward 5-hydroxymethylfurfural and benzyl alcohols for bioprocessing. ACS Catal 10(5):3042–3058. https://doi.org/10.1021/acscatal.9b04727
40. Cleveland M, Lafond M, Xia FR, Chung R, Mulyk P, Hein JE, Brumer H (2021) Two *Fusarium* copper radical oxidases with high activity on aryl alcohols. Biotechnol Biofuels 14(1):138. https://doi.org/10.1186/s13068-021-01984-0
41. Bissaro B, Kodama S, Hage H, Ribeaucourt D, Haon M, Grisel S, Simaan A, Beisson F, Forget S, Brumer H, Rosso M-N, O'Connell R, Lafond M, Kubo Y, Berrin J-G (2021) Unravelling the role of alcohol copper radical oxidases in fungal plant pathogens. https://doi.org/10.21203/rs.3.rs-493001/v1
42. Roberts GP, Gupta SK (1965) Use of galactose oxidase in the histochemical examination of mucus-secreting cells. Nature 207(4995):425–426. https://doi.org/10.1038/207425a0
43. Heitzmann H, Richards FM (1974) Use of the avidin-biotin complex for specific staining of biological membranes in electron microscopy. Proc Natl Acad Sci USA 71(9):3537–3541. https://doi.org/10.1073/pnas.71.9.3537
44. Wilchek M, Spiegel S, Spiegel Y (1980) Fluorescent reagents for the labeling of glycoconjugates in solution and on cell surfaces. Biochem Biophys Res Commun 92(4):1215–1222. https://doi.org/10.1016/0006-291X(80)90416-7
45. Ramya TNC, Weerapana E, Cravatt BF, Paulson JC (2012) Glycoproteomics enabled by tagging sialic acid- or galactose-terminated glycans. Glycobiology 23(2):211–221. https://doi.org/10.1093/glycob/cws144
46. Monosik R, Stredansky M, Tkac J, Sturdik E (2012) Application of enzyme biosensors in analysis of food and beverages. Food Anal Methods 5(1):40–53. https://doi.org/10.1007/s12161-011-9222-4
47. Schoevaart R, Kieboom T (2004) Application of galactose oxidase in chemoenzymatic one-pot cascade reactions without intermediate recovery steps. Top Catal 27(1):3–9. https://doi.org/10.1023/B:TOCA.0000013536.27551.13
48. Mikkonen KS, Parikka K, Suuronen J-P, Ghafar A, Serimaa R, Tenkanen M (2014) Enzymatic oxidation as a potential new route to produce polysaccharide aerogels. RSC Adv 4(23):11884–11892. https://doi.org/10.1039/C3RA47440B
49. Leppänen A-S, Xu C, Parikka K, Eklund P, Sjöholm R, Brumer H, Tenkanen M, Willför S (2014) Targeted allylation and propargylation of galactose-containing polysaccharides in water. Carbohydr Polym 100:46–54. https://doi.org/10.1016/j.carbpol.2012.11.053
50. Leppänen A-S, Niittymäki O, Parikka K, Tenkanen M, Eklund P, Sjöholm R, Willför S (2010) Metal-mediated allylation of enzymatically oxidized methyl α-D-galactopyranoside. Carbohydr Res 345(18):2610–2615. https://doi.org/10.1016/j.carres.2010.09.026
51. Yalpani M, Hall LD (1982) Some chemical and analytical aspects of polysaccharide modifications. II. A high-yielding, specific method for the chemical derivatization of galactose-containing polysaccharides: Oxidation with galactose oxidase followed by reductive amination. J Polym Sci, Polym Chem Ed 20(12):3399–3420. https://doi.org/10.1002/pol.1982.170201213
52. Kelleher FM, Bhavanandan VP (1986) Preparation and characterization of beta-D-fructofuranosyl *O*-(alpha-D-galactopyranosyl uronic acid)-(1–6)-*O*-alpha-D-glucopyranoside and *O*-(alpha- D -galactopyranosyl uronic acid)-(1–6)- D-glucose. Carbohydr Res 155:89–97. https://doi.org/10.1016/S0008-6215(00)90135-6
53. Xu C, Spadiut O, Araújo AC, Nakhai A, Brumer H (2012) Chemo-enzymatic assembly of clickable cellulose surfaces via multivalent polysaccharides. Chemsuschem 5(4):661–665. https://doi.org/10.1002/cssc.201100522
54. Parikka K, Leppänen A-S, Xu C, Pitkänen L, Eronen P, Österberg M, Brumer H, Willför S, Tenkanen M (2012) Functional and anionic cellulose-interacting polymers by selective chemo-enzymatic carboxylation of galactose-containing polysaccharides. Biomacromol 13(8):2418–2428. https://doi.org/10.1021/bm300679a
55. Huffman MA, Fryszkowska A, Alvizo O, Borra-Garske M, Campos KR, Canada KA, Devine PN, Duan D, Forstater JH, Grosser ST, Halsey HM, Hughes GJ, Jo J, Joyce LA, Kolev JN, Liang J, Maloney KM, Mann BF, Marshall NM, McLaughlin M, Moore JC, Murphy GS, Nawrat CC, Nazor J, Novick S, Patel NR, Rodriguez-Granillo A, Robaire SA, Sherer EC, Truppo MD, Whittaker AM, Verma D, Xiao L, Xu Y, Yang H (2019) Design of an in vitro biocatalytic cascade for the manufacture of islatravir. Science 366(6470):1255–1259. https://doi.org/10.1126/science.aay8484
56. Ribeaucourt D, Bissaro B, Guallar V, Yemloul M, Haon M, Grisel S, Alphand V, Brumer H, Lambert F, Berrin J-G, Lafond M (2021) Comprehensive insights into the production of long chain aliphatic aldehydes using a copper-radical alcohol oxidase as biocatalyst. ACS Sustainable Chem Eng 9(12):4411–4421. https://doi.org/10.1021/acssuschemeng.0c07406
57. Rosatella AA, Simeonov SP, Frade RFM, Afonso CAM (2011) 5-Hydroxymethylfurfural (HMF) as a building block platform: biological properties, synthesis and synthetic applications. Green Chem 13(4):754–793. https://doi.org/10.1039/C0GC00401D
58. Sousa AF, Vilela C, Fonseca AC, Matos M, Freire CSR, Gruter G-JM, Coelho JFJ, Silvestre AJD (2015) Biobased polyesters and other polymers from 2,5-furandicarboxylic acid: a tribute to furan excellency. Polym Chem 6(33):5961–5983. https://doi.org/10.1039/C5PY00686D
59. Siebum A, van Wijk A, Schoevaart R, Kieboom T (2006) Galactose oxidase and alcohol oxidase: scope and limitations for the enzymatic synthesis of aldehydes. J Mol Catal B: Enzym 41(3):141–145. https://doi.org/10.1016/j.molcatb.2006.04.003
60. Ribeaucourt D, Bissaro B, Lambert F, Lafond M, Berrin J-G (2021) Biocatalytic oxidation of fatty alcohols into aldehydes for the flavors and fragrances industry. Biotechnol Adv 107787. https://doi.org/10.1016/j.biotechadv.2021.107787
61. Mollerup F, Aumala V, Parikka K, Mathieu Y, Brumer H, Tenkanen M, Master E (2019) A family AA5_2 carbohydrate oxidase from *Penicillium rubens* displays functional overlap across the AA5 family. PLoS One 14(5). https://doi.org/10.1371/journal.pone.0216546
62. Andberg M, Mollerup F, Parikka K, Koutaniemi S, Boer H, Juvonen M, Master E, Tenkanen M, Kruus K (2017) A novel *Colletotrichum graminicola* raffinose oxidase in the AA5 Family. Appl Environ Microbiol 83(20):e01383–e1417. https://doi.org/10.1128/AEM.01383-17
63. Faria CB, de Castro FF, Martim DB, Abe CAL, Prates KV, de Oliveira MAS, Barbosa-Tessmann IP (2019) Production of galactose oxidase inside the *Fusarium fujikuroi* species complex and recombinant expression and characterization of the galactose oxidase GaoA protein from *Fusarium subglutinans*. Mol Biotechnol 61(9):633–649. https://doi.org/10.1007/s12033-019-00190-6
64. Paukner R, Staudigl P, Choosri W, Haltrich D, Leitner C (2015) Expression, purification, and characterization of galactose oxidase of *Fusarium sambucinum* in *E. coli*. Protein Expression Purif 108:73–79. https://doi.org/10.1016/j.pep.2014.12.010
65. Paukner R, Staudigl P, Choosri W, Sygmund C, Halada P, Haltrich D, Leitner C (2014) Galactose oxidase from *Fusarium oxysporum* - expression in *E. coli* and *P. pastoris* and biochemical characterization. PLoS One 9(6):e100116. https://doi.org/10.1371/journal.pone.0100116
66. Whittaker JW (2005) The radical chemistry of galactose oxidase. Arch Biochem Biophys 433(1):227–239. https://doi.org/10.1016/j.abb.2004.08.034
67. Leuthner B, Aichinger C, Oehmen E, Koopmann E, Müller O, Müller P, Kahmann R, Bölker M, Schreier PH (2005) A

H_2O_2-producing glyoxal oxidase is required for filamentous growth and pathogenicity in *Ustilago maydis*. Mol Genet Genomics 272(6):639–650. https://doi.org/10.1007/s00438-004-1085-6
68. Kersten PJ, Cullen D (1993) Cloning and characterization of cDNA encoding glyoxal oxidase, a H_2O_2-producing enzyme from the lignin-degrading basidiomycete *Phanerochaete chrysosporium*. Proc Natl Acad Sci U S A 90(15):7411–7413. https://doi.org/10.1073/pnas.90.15.7411
69. Sun L, Bulter T, Alcalde M, Petrounia IP, Arnold FH (2002) Modification of galactose oxidase to introduce glucose 6-oxidase activity. ChemBioChem 3(8):781–783. https://doi.org/10.1002/1439-7633(20020802)3:8%3c781::AID-CBIC781%3e3.0.CO;2-8
70. Sun L, Petrounia IP, Yagasaki M, Bandara G, Arnold FH (2001) Expression and stabilization of galactose oxidase in *Escherichia coli* by directed evolution. Protein Eng, Des Sel 14(9):699–704. https://doi.org/10.1093/protein/14.9.699
71. Deacon SE, McPherson MJ (2011) Enhanced expression and purification of fungal galactose oxidase in *Escherichia coli* and use for analysis of a saturation mutagenesis library. ChemBioChem 12(4):593–601. https://doi.org/10.1002/cbic.201000634
72. Deacon SE, Mahmoud K, Spooner RK, Firbank SJ, Knowles PF, Phillips SEV, McPherson MJ (2004) Enhanced fructose oxidase activity in a galactose oxidase variant. ChemBioChem 5(7):972–979. https://doi.org/10.1002/cbic.200300810
73. Rogers MS, Tyler EM, Akyumani N, Kurtis CR, Spooner RK, Deacon SE, Tamber S, Firbank SJ, Mahmoud K, Knowles PF, Phillips SEV, McPherson MJ, Dooley DM (2007) The stacking tryptophan of galactose oxidase: a second-coordination sphere residue that has profound effects on tyrosyl radical behavior and enzyme catalysis. Biochemistry 46(15):4606–4618. https://doi.org/10.1021/bi062139d
74. Wilkinson D, Akumanyi N, Hurtado-Guerrero R, Dawkes H, Knowles PF, Phillips SEV, McPherson MJ (2004) Structural and kinetic studies of a series of mutants of galactose oxidase identified by directed evolution. Protein Eng, Des Sel 17(2):141–148. https://doi.org/10.1093/protein/gzh018
75. Escalettes F, Turner NJ (2008) Directed evolution of galactose oxidase: generation of enantioselective secondary alcohol oxidases. ChemBioChem 9(6):857–860. https://doi.org/10.1002/cbic.200700689
76. Rannes JB, Ioannou A, Willies SC, Grogan G, Behrens C, Flitsch SL, Turner NJ (2011) Glycoprotein labeling using engineered variants of galactose oxidase obtained by directed evolution. J Am Chem Soc 133(22):8436–8439. https://doi.org/10.1021/ja2018477
77. Lippow SM, Moon TS, Basu S, Yoon S-H, Li X, Chapman BA, Robison K, Lipovšek D, Prather KLJ (2010) Engineering enzyme specificity using computational design of a defined-sequence library. Chem Biol 17(12):1306–1315. https://doi.org/10.1016/j.chembiol.2010.10.012
78. Gilbert HJ, Knox JP, Boraston AB (2013) Advances in understanding the molecular basis of plant cell wall polysaccharide recognition by carbohydrate-binding modules. Curr Opin Struct Biol 23(5):669–677. https://doi.org/10.1016/j.sbi.2013.05.005
79. Spadiut O, Olsson L, Brumer H (2010) A comparative summary of expression systems for the recombinant production of galactose oxidase. Microb Cell Fact 9(1):68. https://doi.org/10.1186/1475-2859-9-68
80. Whittaker MM, Ballou DP, Whittaker JW (1998) Kinetic isotope effects as probes of the mechanism of galactose oxidase. Biochemistry 37(23):8426–8436. https://doi.org/10.1021/bi980328t
81. Avigad G, Amaral D, Asensio C, Horecker BL (1962) The D-galactose oxidase of *Polyporus circinatus*. J Biol Chem 237(9):2736–2743. https://doi.org/10.1016/S0021-9258(18)60220-0
82. Cooper JAD, Smith W, Bacila M, Medina H (1959) Galactose oxidase from *Polyporus circinatus*, Fr. J Biol Chem 234(3):445–448. https://doi.org/10.1016/S0021-9258(18)70223-8
83. Whittaker MM, Whittaker JW (1988) The active site of galactose oxidase. J Biol Chem 263(13):6074–6080. https://doi.org/10.1016/S0021-9258(18)68751-4
84. Xu F, Golightly EJ, Schneider P, Berka RM, Brown KM, Johnstone JA, Baker DH, Fuglsang CC, Brown SH, Svendsen A, Klotz AV (2000) Expression and characterization of a recombinant *Fusarium spp.* galactose oxidase. Appl Biochem Biotechnol 88(1):23. https://doi.org/10.1385/ABAB:88:1-3:023
85. Henrissat B, Teeri TT, Warren RA (1998) A scheme for designating enzymes that hydrolyse the polysaccharides in the cell walls of plants. FEBS Lett 425(2):352–354. https://doi.org/10.1016/S0014-5793(98)00265-8
86. Whittaker MM, Whittaker JW (2001) Catalytic reaction profile for alcohol oxidation by galactose oxidase. Biochemistry 40(24):7140–7148. https://doi.org/10.1021/bi0103031
87. Carro J, Ferreira P, Rodríguez L, Prieto A, Serrano A, Balcells B, Ardá A, Jiménez-Barbero J, Gutiérrez A, Ullrich R, Hofrichter M, Martínez AT (2015) 5-hydroxymethylfurfural conversion by fungal aryl-alcohol oxidase and unspecific peroxygenase. FEBS J 282(16):3218–3229. https://doi.org/10.1111/febs.13177
88. Forget SM, Xia F, Hein JE, Brumer H (2020) Determination of biocatalytic parameters of a copper radical oxidase using real-time reaction progress monitoring. Org Biomol Chem 18(11):2076–2084. https://doi.org/10.1039/C9OB02757B
89. Toftgaard Pedersen A, Birmingham WR, Rehn G, Charnock SJ, Turner NJ, Woodley JM (2015) Process requirements of galactose oxidase catalyzed oxidation of alcohols. Org Process Res Dev 19(11):1580–1589. https://doi.org/10.1021/acs.oprd.5b00278
90. Pagliaro M, Rossi M (2010) Glycerol: Properties and production. The Future of Glycerol. Royal Society of Chemistry's, Cambridge, UK. https://doi.org/10.1039/9781849731089
91. Klibanov AM, Alberti BN, Marletta MA (1982) Stereospecific oxidation of aliphatic alcohols catalyzed by galactose oxidase. Biochem Biophys Res Commun 108(2):804–808. https://doi.org/10.1016/0006-291X(82)90900-7
92. Ito N, Phillips SEV, Yadav KDS, Knowles PF (1994) Crystal structure of a free radical enzyme, Galactose Oxidase. J Mol Biol 238(5):794–814. https://doi.org/10.1006/jmbi.1994.1335
93. Chaplin AK, Petrus MLC, Mangiameli G, Hough MA, Svistunenko DA, Nicholls P, Claessen D, Vijgenboom E, Worrall JAR (2015) GlxA is a new structural member of the radical copper oxidase family and is required for glycan deposition at hyphal tips and morphogenesis of *Streptomyces lividans*. Biochem J 469(3):433–444. https://doi.org/10.1042/bj20150190
94. Chaplin AK, Svistunenko DA, Hough MA, Wilson MT, Vijgenboom E, Worrall JA (2017) Active-site maturation and activity of the copper-radical oxidase GlxA are governed by a tryptophan residue. Biochem J 474(5):809–825. https://doi.org/10.1042/bcj20160968
95. Dijkman WP, Fraaije MW (2014) Discovery and Characterization of a 5-Hydroxymethylfurfural Oxidase from *Methylovorus* sp. Strain MP688. Appl Environ Microbiol 80(3):1082–1090. https://doi.org/10.1128/AEM.03740-13
96. Kadowaki MAS, Godoy MOd, Kumagai PS, Costa-Filho AJd, Mort A, Prade RA, Polikarpov I (2018) Characterization of a new glyoxal oxidase from the thermophilic fungus *Myceliophthora thermophila* M77: Hydrogen peroxide production retained in 5-Hydroxymethylfurfural oxidation. Catalysts 8(10):476. https://doi.org/10.3390/catal8100476

97. Daou M, Yassine B, Wikee S, Record E, Duprat F, Bertrand E, Faulds CB (2019) *Pycnoporus cinnabarinus* glyoxal oxidases display differential catalytic efficiencies on 5-hydroxymethylfurfural and its oxidized derivatives. Fungal Biol Biotechnol 6(1):4. https://doi.org/10.1186/s40694-019-0067-8
98. Grigoriev IV, Cullen D, Goodwin SB, Hibbett D, Jeffries TW, Kubicek CP, Kuske C, Magnuson JK, Martin F, Spatafora JW, Tsang A, Baker SE (2011) Fueling the future with fungal genomics. Mycology 2(3):192–209. https://doi.org/10.1080/21501203.2011.584577
99. Grigoriev IV, Nikitin R, Haridas S, Kuo A, Ohm R, Otillar R, Riley R, Salamov A, Zhao X, Korzeniewski F, Smirnova T, Nordberg H, Dubchak I, Shabalov I (2013) MycoCosm portal: gearing up for 1000 fungal genomes. Nucleic Acids Res 42(D1):D699–D704. https://doi.org/10.1093/nar/gkt1183
100. Katoh K, Standley DM (2013) MAFFT multiple sequence alignment software version 7: improvements in performance and usability. Mol Biol Evol 30(4):772–780. https://doi.org/10.1093/molbev/mst010
101. Miller MA, Pfeiffer W, Schwartz T (2010) Creating the CIPRES Science Gateway for inference of large phylogenetic trees. 2010 Gateway Computing Environments Workshop (GCE). https://doi.org/10.1109/GCE.2010.5676129.
102. Stamatakis A (2014) RAxML version 8: a tool for phylogenetic analysis and post-analysis of large phylogenies. Bioinformatics 30(9):1312–1313. https://doi.org/10.1093/bioinformatics/btu033
103. Camacho C, Coulouris G, Avagyan V, Ma N, Papadopoulos J, Bealer K, Madden TL (2009) BLAST+: architecture and applications. BMC Bioinf 10(1):421. https://doi.org/10.1186/1471-2105-10-421
104. Shannon P, Markiel A, Ozier O, Baliga NS, Wang JT, Ramage D, Amin N, Schwikowski B, Ideker T (2003) Cytoscape: a software environment for integrated models of biomolecular interaction networks. Genome Res 13(11):2498–2504. https://doi.org/10.1101/gr.1239303
105. Kelley LA, Mezulis S, Yates CM, Wass MN, Sternberg MJE (2015) The Phyre2 web portal for protein modeling, prediction and analysis. Nat Protoc 10(6):845–858. https://doi.org/10.1038/nprot.2015.053
106. Haon M, Grisel S, Navarro D, Gruet A, Berrin J-G, Bignon C (2015) Recombinant protein production facility for fungal biomass-degrading enzymes using the yeast *Pichia pastoris*. Front Microbiol 6(1002). https://doi.org/10.3389/fmicb.2015.01002
107. Re R, Pellegrini N, Proteggente A, Pannala A, Yang M, Rice-Evans C (1999) Antioxidant activity applying an improved ABTS radical cation decolorization assay. Free Radical Biol Med 26(9):1231–1237. https://doi.org/10.1016/S0891-5849(98)00315-3
108. Pettersen EF, Goddard TD, Huang CC, Couch GS, Greenblatt DM, Meng EC, Ferrin TE (2004) UCSF Chimera—a visualization system for exploratory research and analysis. J Comput Chem 25(13):1605–1612. https://doi.org/10.1002/jcc.20084
109. Trott O, Olson AJ (2010) AutoDock Vina: improving the speed and accuracy of docking with a new scoring function, efficient optimization, and multithreading. J Comput Chem 31(2):455–461. https://doi.org/10.1002/jcc.21334
110. Daou M, Piumi F, Cullen D, Record E, Faulds CB (2016) Heterologous production and characterization of two glyoxal oxidases from *Pycnoporus cinnabarinus*. Appl Environ Microbiol 82(16):4867–4875. https://doi.org/10.1128/AEM.00304-16
111. Cordeiro FA, Faria CB, Barbosa-Tessmann IP (2010) Identification of new galactose oxidase genes in *Fusarium* spp. J Basic Microbiol 50(6):527–537. https://doi.org/10.1002/jobm.201000078